Lithos 336–337 (2019) 27–39

Contents lists available at ScienceDirect

Lithos

journal homepage: www.elsevier.com/locate/lithos

An effect of reduced S-rich fluids on diamond formation under mantle-slab interaction

Yuliya V. Bataleva [a,*], Yuri N. Palyanov [a,b], Yuri M. Borzdov [a], Ivan D. Novoselov [a,b], Oleg A. Bayukov [c]

[a] Sobolev Institute of Geology and Mineralogy, Siberian Branch of the Russian Academy of Sciences, Academican Koptyug Ave., 3, Novosibirsk 630090, Russian Federation
[b] Novosibirsk State University, Pirogova str., 2, Novosibirsk 630090, Russian Federation
[c] Kirensky Institute of Physics, Siberian Branch of Russian Academy of Sciences, Akademgorodok 50, bld. 38, Krasnoyarsk 660036, Russian Federation

ARTICLE INFO

Article history:
Received 24 November 2018
Accepted 24 March 2019
Available online 27 March 2019

Keywords:
Sulfur-rich fluid
Iron carbide
Diamond
Mantle sulfides
High-pressure experiment

ABSTRACT

Experimental study, dedicated to understanding the effect of S-rich reduced fluids on the diamond-forming processes under subduction settings, was performed using a multi-anvil high-pressure split-sphere apparatus in Fe_3C-$(Mg,Ca)CO_3$-S and Fe^0-$(Mg,Ca)CO_3$-S systems at the pressure of 6.3 GPa, temperatures in the range of 900–1600 °C and run time of 18–60 h. At the temperatures of 900 and 1000 °C in the carbide-carbonate-sulfur system, extraction of carbon from cohenite through the interaction with S-rich reduced fluid, as well as C^0-producing redox reactions of carbonate with carbide were realized. As a result, graphite formation in assemblage with magnesiowüstite, cohenite and pyrrhotite (±aragonite) was established. At higher temperatures (≥1100 °C) formation of assemblage of Fe^{3+}-magnesiowüstite and graphite was accompanied by generation of fO_2-contrasting melts - metal-sulfide with dissolved carbon (Fe-S-C) and sulfide-oxide (Fe-S-O). In the temperature range of 1400–1600 °C spontaneous diamond nucleation was found to occur via redox interactions of carbide or iron with carbonate. It was established, that interactions of Fe-S-C and Fe-S-O melts as well as of Fe-S-C melt and magnesiowüstite, were C^0-forming processes, accompanied by disproportionation of Fe. These resulted in the crystallization of Fe^{3+}-magnesiowüstite+graphite assemblage and growth of diamond. We show that a participation of sulfur in subduction-related elemental carbon-forming processes results in sharp decrease of partial melting temperatures (~300 °C), reducting the reactivity of the Fe-S-C melt relatively to Fe—C melt with respect to graphite and diamond crystallization and decrease of diamond growth rate.

1. Introduction

Modern data regarding global geochemical cycles of carbon and sulfur, demonstrate that subduction of crustal material plays a key role in transportation of C– and S-bearing minerals such as carbonates, hydrocarbons, sulfates and sulfides, into the deep mantle (Dilek and Yang, 2018; Dobrzhinetskaya et al., 2007; Evans, 2012; Luth, 1999; Sobolev and Sobolev, 1980). Behavior patterns of carbon and sulfur, as redox-sensitive elements, having a strong impact on the mantle igneous and metasomatic processes, the redox evolution of the Earth's mantle, as well as on the processes of fluid generation, diamond formation and mantle sulfide genesis, are of continuing interest.

Carbonates, which are the main form of carbon storage in the subducted material, are supposed to be thermodynamically stable down to P-T conditions of the lower mantle (Oganov et al., 2008). Most carbonates (up to 80%) are believed to survive subduction-related decarbonation, dehydration or melting (Dasgupta and Hirschmann, 2010; Yaxley and Green, 1994) and can transport to depths >600 km (Shirey et al., 2013; Walter et al., 2011). Direct evidence of the presence of carbonates in the Earth's mantle have been provided by carbonate inclusions in diamonds (Brenker et al., 2007; Kaminsky et al., 2013; Logvinova et al., 2015; Stachel et al., 1998; Wang et al., 1996; Wirth et al., 2009).

A number of modern researches, including experimental modeling (Rohrbach et al., 2007; Rohrbach and Schmidt, 2011), oxythermobarometry of mantle rocks (Frost and McCammon, 2008; Stagno et al., 2011; Woodland and Koch, 2003) and theoretical modeling of the mantle fO_2 evolution (Ballhaus, 1995) predicts that mantle likely becomes more reduced with depth, resulting in Fe—Ni metal saturation below 250 ± 30 km. Existence of metal-saturated mantle rocks is confirmed by the presence of metallic iron, iron-nickel alloys and iron carbides as diamond inclusions (Ballhaus, 1995; Meyer and Svicero, 1975; Smith et al., 2016; Sobolev et al., 1981; Stachel et al., 1998; Wirth et al., 2009). Rohrbach and Schmidt (2011) substantiated a potential subduction-related carbonate-metal interaction under reduced mantle conditions. Experimental modeling of interaction processes of reduced metal-saturated mantle rocks with oxidized carbonate-bearing slab, resulted in the formation of diamond, was performed by Palyanov et al. (2013).

* Corresponding author at: Koptyug ave 3, Novosibirsk 630090, Russian Federation.
E-mail address: bataleva@igm.nsc.ru (Y.V. Bataleva).

https://doi.org/10.1016/j.lithos.2019.03.027
0024-4937/

As mentioned above, S-bearing minerals (sulfates and sulfides) are very characteristic for subduction environments (Evans, 2012). Moreover, sulfur is supposed to be a common component of mantle metasomatic agents, such as C-O-H-S fluids, sulfide melts or silicate melts with dissolved sulfur (Evans, 2012). Although down-going slab is the most probable source of these agents, mantle plumes (e.g. Schissel and Smail, 2001) and various processes at the Earth's core-lower mantle boundary, resulting in partial melting events (Haggerty, 1986; Wood et al., 2014) can also be proposed as sources of S-rich melts or fluids. Under redox conditions characteristic for subcratonic mantle peridotites, S-bearing fluids are supposed to be of H_2S composition (reduced) rather than SO_2 (oxidized) (Eggler and Lorand, 1993), which confirms the possibility of interaction between deep mantle metal-saturated rocks and S-rich reduced fluids.

Considering that sulfides are extremely widespread as inclusions in diamonds (e.g. Sharp, 1966; Sobolev, 1977; Bulanova, 1995; Deines and Harris, 1995), the role of sulfides and other S-bearing phases in diamond genesis has been explored for many decades. In the 1970s–1980s two different models of the participation of sulfides in the formation of diamond were proposed. One of them implies the crystallization of diamonds from sulfide melt saturated with carbon (Haggerty, 1986) similarly to the synthesis of diamond from a carbon solution in a transitional metal melt. Another model was proposed by Marx (Marx, 1972), who suggested that one of the diamond-forming reactions could be $2FeS + CO_2 = 2FeO + S_2 + C$. In order to perform experimental verification of these reactions, a number of researches in S-bearing systems were made. It was found that pure sulfur can act as solvent-catalyst for diamond crystallization under high P-T conditions (Pal'yanov et al., 2001; Sato and Katsura, 2001). Experimental data on the interaction of sulfide melt with carbon (Litvin et al., 2002; Palyanov et al., 2006; Wentorf, 1974) showed that diamond nucleation and crystallization in sulfide melt can be realized under P-T parameters much higher that those for the formation of most natural diamonds. Although sulfide melts are the least effective diamond-forming medium under mantle conditions compared to carbonate, fluid and carbonate-silicate-fluid (Akaishi et al., 1990; Bureau et al., 2018; Girnis et al., 2018; Pal'yanov et al., 2002, 2005; Sato et al., 1999; Taniguchi et al., 1996), it is now known that they can play a first order role in natural diamond formation processes. It should be noted, that despite potential carbon sources in the processes of natural diamond formation are carbonates, hydrocarbons, CO_2 and carbides, graphite was used as a carbon source in most experimental studies on diamond formation. Thus, the ideas of Marx, mentioned above, are much more probable to be realized in natural conditions. It was experimentally established that sulfides can act as reducing agents for CO_2-fluid, providing conditions for the crystallization of diamond (or graphite) from carbon of carbonates as a result of redox reactions (Gunn and Luth, 2006; Palyanov et al., 2007). Moreover, experimental modeling of the interaction of sulfide melt or S-rich reduced fluid with iron carbide (Bataleva et al., 2017) showed that both can implement extraction of carbon from Fe_3C leading to the formation of graphite and diamond. The recent study of Smith et al. (2016) demonstrated that large *gem* diamonds contain inclusions of solidified iron-nickel-carbon-sulfur melt, accompanied by a reduced fluid, which are direct evidence of crystallization from a redox-sensitive metallic liquid phase in the deep mantle. These sublithospheric diamonds display isotopically light carbon compositions, which are thought to result from recycling of crystal carbon, i.e. evidence their subduction origin.

In the present study we report new experimental modeling results on the effect of S-rich reduced fluid on the formation of elemental carbon (diamond and graphite) in the course of interaction of reduced metal-saturated mantle with oxidized carbonate-bearing slab.

2. Materials and methods

Experimental studies of the effect of reduced sulfur-rich fluids on diamond formation under subduction conditions were performed on a base of carbide-carbonate-sulfur (Fe_3C-$(Mg,Ca)CO_3$-S) and iron-carbonate-sulfur (Fe^0-$(Mg,Ca)CO_3$-S) interactions at the pressure of 6.3 GPa, in a temperature range of 900–1600°C, and with durations of 18 to 60 h, using a high-pressure multi-anvil split-sphere apparatus (BARS) (Pal'yanov et al., 2002). The experiemental protocole, high-pressure cell design, and calibration details were published elsewhere (Pal'yanov et al., 2002; Sokol et al., 2015). Initial materials consisted of natural magnesite and dolomite with an impurity content of <0.5 wt% (~0.2 wt% FeO and ~0.2 wt% MnO), powders of chemically pure Fe^0 and S (99.999%), and pre-synthesized cohenite (Fe_3C). Cohenite was preliminarily synthesized in a Fe—C system at P = 5.7 GPa and T = 1450 °C, and thoroughly analyzed by X-Ray. The initial mixture of carbonates had a bulk composition of $Mg_{0.9}Ca_{0.1}CO_3$. Weight proportions of the initial materials are shown in Table 1. All these materials were finely powdered to a particle size <20 μm, mixed, and thoroughly homogenized. To avoid absorption of atmospheric water by carbonate after grinding, powdered carbonates were dried at a temperature of ~160°C for 120 h. When assembling ampoules for experiments in the carbide-carbonate-sulfur system, a part of the initial carbide was not ground, but was added to the mixture as 300–400 μm crystal fragments, to enable reconstruction of the interaction of carbide with carbonate phases and sulfur. Seed diamond crystals of a cubo-octahedral habit (~500 μm in size) were placed into the ampoule to obtain information on diamond growth at temperatures lower than required for spontaneous diamond nucleation. Diamond seed crystals were thoroughly selected and examined before and after experiments. More specifically, we used only diamonds with smooth faces, weighted before and after the experiments to reveal either weight loss or increase; micro morphology of every seed was studied after the experiments to determine growth or dissolution patterns, heterogeneous diamond nucleation, graphitization or formation of amorphous carbon on the diamond seed faces.

Based on previous experiments dealing with sulfides and sulfur at mantle P and T, graphite was chosen as the optimal capsule material. In addition, the graphite capsule acts as an outer buffer, setting an upper limit of fO_2 values in the sample close to the CCO equilibrium during experiments (Palyanov et al., 2007). We also performed a control series of experiments using talc ceramics and MgO as the capsule material (Table 2). Capsules made from these materials were found not to provide the composition stability (Table 2) and mass balance for Fe^0-$(Mg,Ca)CO_3$-S and Fe_3C-$(Mg,Ca)CO_3$-S systems at experimental P-T parameters. However, their use demonstrated that the iron-carbonate-sulfur and carbide-carbonate-sulfur interactions were effective for graphite formation under conditions of non-graphite sources of carbon (alkaline earth carbonate and iron carbide).

The phase and chemical compositions of produced samples were determined using microprobe analysis (Camebax-micro) and energy dispersive spectroscopy (Tescan MIRA3 LMU scanning electron microscope). Microprobe and EDS analyses of sulfide, silicate, oxide, and carbide mineral phases were performed at an accelerating voltage of 20 kV, a probe current of 20 nA, a counting time of 10 s on each analytical line, and an electron beam probe diameter of 2–4 μm. In the case of carbonates and quenched melts, we reduced the accelerating voltage to 15 kV, the probe current to 10 nA, the counting time to 10 s and used a defocused beam (20–100 μm in diameter). Natural magnesite, calcite,

Table 1
Mass proportions of starting materials and bulk compositions of the iron-carbonate-sulfur and carbide-carbonate-sulfur systems.

System	Starting materials, mg					Mass concentrations, wt%						
	Ms	Dol	Fe^0	Fe_3C	S	Fe	Mg	Mn	Ca	C	S	O
Fe^0-$(Mg,Ca)CO_3$-S	14	8	43	–	8	58.9	6.9	<<0.1	2.4	4.2	11.0	16.7
Fe_3C-$(Mg,Ca)CO_3$-S	14	8	–	45	8	56.0	6.7	<<0.1	2.3	8.1	10.7	16.2

Table 2
Experimental parameters and results in the carbide-carbonate-sulfur and iron-carbonate-sulfur systems at P = 6.3 GPa.

Run no.	T, °C	t, h	Capsule material	Final phases		
				Carbide, carbonate, sulfide, oxide	Carbon phases	Melts
				Fe_3C-$(Mg,Ca)CO_3$-S		
CCS-23	900	18	Gr	Po, Mws, Arg, Ms., Dol, Coh	Gr, D_{NC}	–
CCS-03	1000	18	Gr	Po, Mws, Arg, Coh	Gr, D_{NC}	–
CCS-20	1100	18	Gr	Po, Mws	Gr, D_{NC}	$L_{Fe\text{-}S\text{-}C}$, $L_{Fe\text{-}S\text{-}O}$
CCS-19	1200	18	Gr	Po, Mws	Gr, D_{NC}	$L_{Fe\text{-}S\text{-}C}$, $L_{Fe\text{-}S\text{-}O}$
CCS-99	1300	18	Gr	Mws	Gr, D_{NC}	$L_{Fe\text{-}S\text{-}C}$, $L_{Fe\text{-}S\text{-}O}$
CCS-18	1400	18	Gr	Mws	Gr, DG, Dm	$L_{Fe\text{-}S\text{-}C}$, $L_{Fe\text{-}S\text{-}O}$
CCS-96	1500	18	Gr	Mws	Gr, DG, Dm	$L_{Fe\text{-}S\text{-}C}$, $L_{Fe\text{-}S\text{-}O}$
CCS-02	1600	18	Gr	Mws	Gr, DG, Dm	$L_{Fe\text{-}S\text{-}C}$, $L_{Fe\text{-}S\text{-}O}$
CCS-93	1100	20	Ta	Po, Mws	Gr	–
CCS-92	1200	20	Ta	Po, Mws, Ol	Gr	–
CCS-86	1400	18	MgO	Po, Mws, Fpc	Gr, DG	$L_{Fe\text{-}S\text{-}C}$, $L_{Fe\text{-}S\text{-}O}$
				Fe^0-$(Mg,Ca)CO_3$-S		
MCS-98	1500	18	Gr	Mws	Gr, DG, Dm	$L_{Fe\text{-}S\text{-}C}$, $L_{Fe\text{-}S\text{-}O}$
MCS-02	1600	18	Gr	Mws	Gr, DG, Dm	$L_{Fe\text{-}S\text{-}C}$, $L_{Fe\text{-}S\text{-}O}$

Po – pyrrhotite, Mws – magnesiowustite, Coh – cohenite, Arg – aragonite, Ms – magnesite, Dol – dolomite, Gr – metastable graphite, D_{NC} – no changes on diamond seeds, DG – diamond growth on seeds, Dm – spontaneously nucleated diamond, Ol – olivine, Ta – talc, $L_{Fe\text{-}S\text{-}C}$ – Fe-S-C melt, $L_{Fe\text{-}S\text{-}O}$ – Fe-S-O melt, Fpc – ferropericlase.

pyrrhotite, pyrite, metallic iron, and carbide were used as standards. Phase relationships in samples were investigated by scanning electron microscopy. Micro-Raman spectra were recorded on a Horiba Jobin Yvon LabRAM HR800 spectrometer equipped with an Olympus BX41 microscope. A 325 nm He—Cd laser was used as excitation source. These analytical studies were carried out at the Analytical Center for Multi-Element and Isotope Analysis of the Siberian Branch of the Russian Academy of Sciences. Mass proportions of produced phases were calculated using the mass balance method (least squares method). The composition of iron-bearing phases, their iron valence state, and distribution of iron over phases and nonequivalent positions were analyzed by Mössbauer spectroscopy; measurements were performed at room temperature on a MC-1104 Em spectrometer with a $Co^{57}(Cr)$ source and powder absorber thickness of 1–5 mg/cm^2. Mössbauer spectra were measured at the Kirensky Institute of Physics of the Siberian Branch of the Russian Academy of Sciences.

3. Experimental results

3.1. Carbide-carbonate-sulfur interaction

The results of experiments in the carbide-carbonate-sulfur system as well as the phases compositions are shown in Tables 2–5. In the carbide-carbonate-sulfur system at the lowest temperatures (900 and 1000 °C), pyrrhotite, magnesiowüstite, graphite, and aragonite are formed, and single crystals of starting carbide and Mg,Ca-carbonates are preserved. The predominant phases in produced samples are pyrrhotite ($Fe_{0.98–0.99}S$) and magnesiowüstite ($Fe_{0.69–0.75}Mg_{0.25–0.31}O$) (Fig. 1a).

The formation of three types of reaction (zonal) assemblages was observed at the contact of preserved single crystals of cohenite, magnesite, and dolomite with newly formed pyrrhotite. The first type is graphite rims around cohenite crystals (Fig. 1a), which are similar to those described earlier (Bataleva et al., 2017) for carbide-sulfur and carbide-sulfide systems. The second type is reaction rims of a microcrystalline aggregate represented by regular inter-growths of graphite and magnesiowüstite around magnesite (Fig. 1b, c). The third type is a polycrystalline aggregate of aragonite, magnesiowüstite, and graphite, which partially or completely replaces initial dolomite crystals (Fig. 1d). It should be noted that magnesiowüstite formed in this temperature range has a homogeneous composition (Mg# 0.25–0.30) within each sample and always occurs in association with graphite in the form of regular inter-growths, microcrystalline aggregates, or inclusions. Mössbauer spectroscopy revealed that magnesiowüstite contained ferric iron (Table 5) with $Fe^{3+}/\Sigma Fe$ ~ 0.07.

At 1100 °C, the solid phase association of pyrrhotite + magnesiaustite + graphite and the first portions of Fe-S-C and Fe-S-O melts formed in the carbide-carbonate-sulfur system (Fig. 2). In a temperature range of 1200–1600 °C, samples lack pyrrhotite, and the phase association is represented by magnesiowüstite, graphite (±diamond), and Fe-S-C and Fe-S-O melts (Fig. 1e-i). These melts are present in samples in the form of quenched aggregates of pyrrhotite + iron (with dissolved carbon) and pyrrhotite + wüstite (Fig. 1f, g), respectively. Graphite occurs in samples as inter-growths with magnesiowüstite and also forms "relic" reaction rims delineating the boundaries of the initial cohenite grains that have completely reacted during the experiments (Fig. 1e, f). Quenched aggregates of two melts occur inside the graphite rims (Fig. 1f, h). Depending on the temperature, the Fe-S-C melt is characterized by compositions of $Fe_{79}S_{20}C_1$ (1100 °C)–$Fe_{78}S_{19}C_3$ (1600 °C), and the Fe-S-O melt is characterized by compositions of $Fe_{63}S_{35}O_2$ (1100 °C)–$Fe_{64}S_{30}O_6$ (1600 °C) (Table 4). Hereafter, compositions of the Fe-S-C and Fe-S-O melts are presented as weight percentage (wt%). In an interval of 1100–1500 °C, the composition of magnesiowüstite (~$Fe_{0.64}Mg_{0.30}Ca_{0.06}O$) is almost independent of temperature, and $Fe^{3+}/\Sigma Fe$ values amount to 0.06–0.08. At a temperature of 1600 °C, magnesiowüstite occurs as large rounded crystals with a zonal structure: a high-magnesium central part (~$Fe_{0.49}Mg_{0.46}Ca_{0.05}O$, $Fe^{3+}/\Sigma Fe$ ~ 0.07) and high-iron periphery (~$Fe_{0.93}Mg_{0.07}O$, $Fe^{3+}/\Sigma Fe$ ~ 0.12) (Table 3).

The spontaneous formation of diamond due to the carbide-carbonate-sulfur interaction and the formation of an overgrown layer on seed diamond crystals were observed in a temperature interval of 1400–1600 °C (Figs. 1h-i, 2). The synthesized diamond crystals are predominantly represented by octahedra (10–80 μm) and their inter-growths (up to 120 μm). They are characterized by the presence of magnesiowüstite inclusions (Fig. 1i) and single inclusions of a sulfide melt. Diamond crystals are situated in a polycrystalline magnesiowüstite + graphite aggregate directly at the contact with quenched Fe-S-C and Fe-S-O melts. Nucleation centers are uniformly distributed in the bulk sample, and their number ranges from ~10/mm^3 (1400 °C) to ~15/mm^3 (1600 °C). The growth rate of spontaneous diamond crystals is about 4 to 5 μm/h.

3.2. Iron-carbonate-sulfur interaction

A detailed description of the interaction in the Fe^0-$(Mg,Ca)CO_3$-S system in an interval of 900–1400 °C was presented by Bataleva et al., 2016. In the present paper, we describe the results of additional experiments carried out at 1500 and 1600 °C. At T ≥ 1500°C formation of solid phase association of magnesiowüstite + graphite + diamond and generation of two melts - Fe-S-C and Fe-S-O (Figs. 2, 3a-c) occur. These

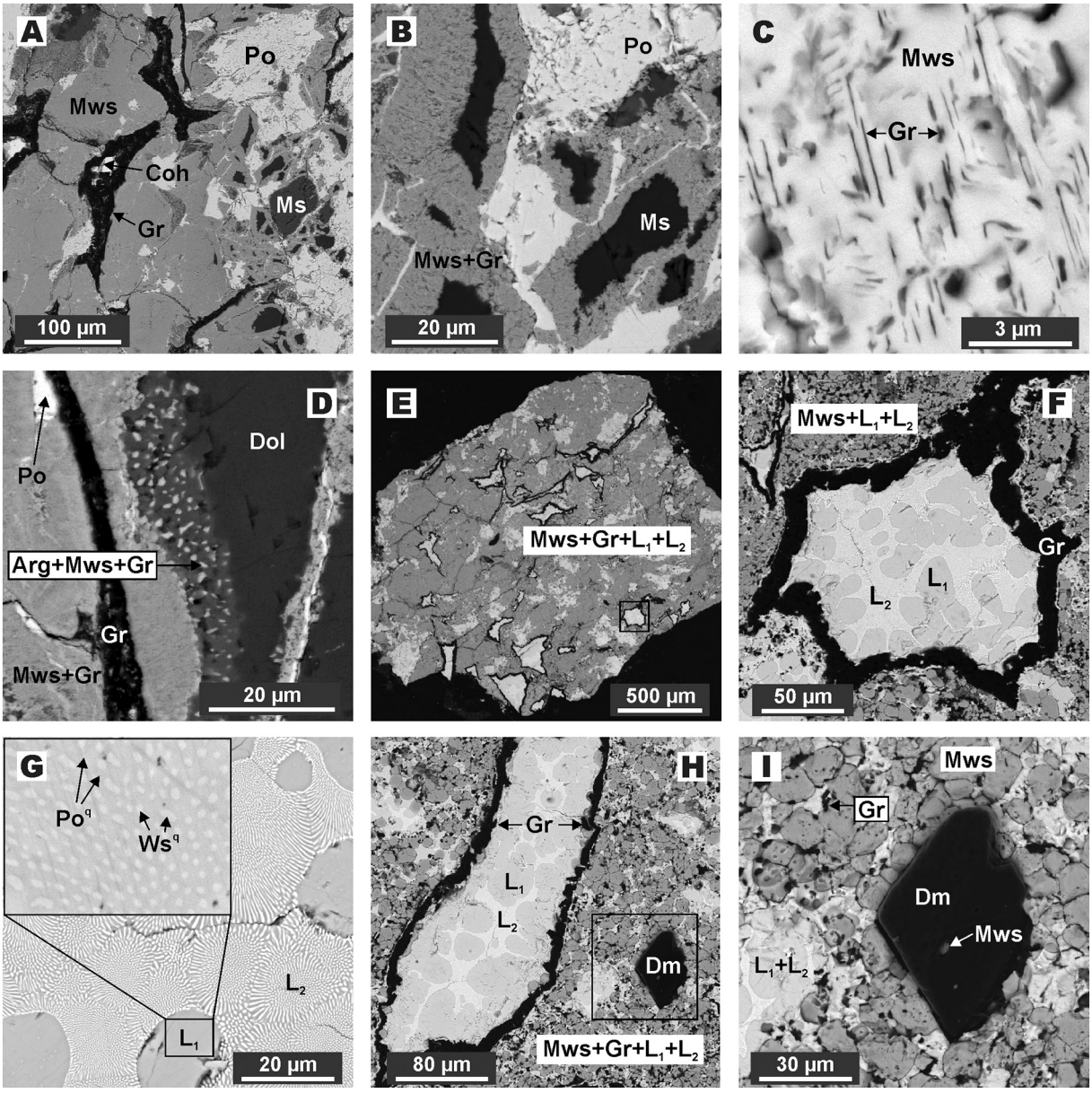

Fig. 1. SEM micrographs (BSE) of polished sections of the samples after experiments in carbide-carbonate-sulfur system, (A-D) - 900 °C, N CCS-23; (E-G) - 1200 °C, N CCS-19; (H—I) - 1400 °C, CCS-18. A - reaction rim of graphite around cohenite in polycrystalline magnesiowüstite + graphite + pyrrhotite aggregate. B - reaction rims of magnesiowüstite+graphite around magnesite crystals. C - parallel graphite micro-plates encapsulated in magmesiowustite. D - reaction rim of aragonite+ magnesiowüstite+graphite at the contact with dolomite. E - overall view of the vertical section of the sample. F - enlarged fragment of Fig. 1F, quenched Fe-S-O and Fe-S-C melts, surrounded by a wide graphite reaction rim. G - structure of quenched Fe-S-O and Fe-S-C melts. H, I - diamond crystal in the polycrystalline aggregate of magnesiowüstite with microdendrite aggregates of quenched Fe-S-C and Fe-S-O melts. Ms - magnesite, Dol - dolomite, Ws - wustite, Mws - magnesiowüstite, Dm - spontaneously nucleated diamond, Gr - metastable graphite, Po - pyrrhotite, Coh - cohenite, L_1 - Fe-S-O melt, L_2 - Fe-S-C melt, ^{q} - quenched phase.

melts are represented by quenched aggregates of pyrrhotite + iron (with dissolved carbon) and pyrrhotite + wüstite (Fig. 3a). Magnesiowüstite produced in this temperature range occurs in quenched aggregates of Fe-S-C and Fe-S-O melts and is represented by rounded crystals with inclusions of graphite plates. Crystals of metastable graphite are also present in large quantities directly in quenched melts (Fig. 3a). The compositions of melts are $Fe_{76}S_{22}C_2$ and $Fe_{64}S_{29}O_7$ (1500 °C)–$Fe_{63}S_{32}O_4$ (1600 °C) (Table 4). At these temperatures, magnesiowüstite crystals are zoned and characterized by a high-magnesium core (~$Fe_{0.51}Mg_{0.44}Ca_{0.06}O$, $Fe^{3+}/\Sigma Fe$ ~0.08) and a high-iron periphery (~$Fe_{0.79–0.83}Mg_{0.17–0.21}O$, $Fe^{3+}/\Sigma Fe$ ~ 0.12) (Figs. 3a, 4; Table 3).

As mentioned above, at temperatures of 1500 and 1600 °C, the iron-carbonate-sulfur interaction leads to spontaneous crystallization of diamond and formation of an overgrown layer on seed diamond crystals (Fig. 2). Spontaneous diamond crystals are mainly represented by octahedra (10–50 μm), flattened octahedra (10–60 μm), and their inter-growths (up to 100 μm) (Fig. 3b, c). The produced diamonds are spatially confined to quenched aggregates of Fe-S-C and Fe-S-O melts and are relatively uniformly distributed in the sample bulk. The number of crystallization centers is about 20/mm^3, and the growth rate amounts to 3–5 μm/h.

3.3. Results of the Raman spectroscopy of graphite and diamond

Structural characterization of graphite and diamond was performed using Raman spectroscopy. The main goals were to estimating the defectiveness of graphite in the polycrystalline rims and single plate crystals, to elucidate the temperature dependencies of Raman features, and to characterize the spontaneously nucleated diamond crystals and

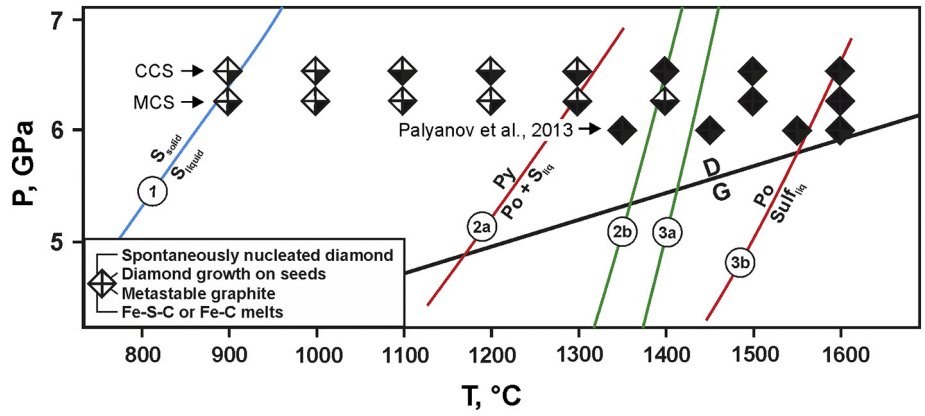

Fig. 2. P-T diagram showing the experimental results of the carbide-carbonate-sulfur (upper row), iron-carbonate-sulfur (this study and Bataleva et al., 2016) (middle row) and iron-carbonate (Palyanov et al., 2013) (lower row) interactions. Symbols are vertically displaced for clarity, all experiments were performed under a pressure of 6.3 GPa and 6.5 GPa (Palyanov et al., 2013). Experimentally determined curves: 1 - melting of sulfur (Brazhkin et al., 1999); 2a, 3a - decomposition of pyrite (Boehler, 1992; Sharp, 1969); 2b, 3b – melting of pyrrhotite (Boehler, 1992; Sharp, 1969); G/D - graphite-to-diamond transformation line after Kennedy and Kennedy, 1976.

inclusions therein. Representative spectra of the graphite and diamond crystals and inclusions therein, synthesized as a result of carbide-carbonate-sulfur interaction, are shown in the Figs. 5–7. Spectra were recorded in the Raman shift range of 1000 to 3500 cm^{-1}. All graphite spectra display the first-order D (1348–1352 cm^{-1}), G (1579–1582 cm^{-1}) and D' (1619–1623 cm^{-1}) bands and second-order G' (2703–2719 cm^{-1}) and D + G (2935–2940 cm^{-1}) bands. First-order bands are represented by narrow and sharp peaks, without any feature of widened peaks, characteristic of sp^3 amorphous carbon.

Graphite from the reaction rims around cohenite crystals is the only form of graphite in the samples obtained in the temperature range of 900 to 1200 °C. At the temperatures of 1300 and 1400 °C formation of both reaction rims and plate crystals occur, and at higher temperatures – only plates of graphite are crystallized. The most characteristic Raman feature for the graphite from rims at 900 °C is the higher intensity of the defect-related D and D' bands relatively to the G-band (Table 6), with I_D/I_G ratio of 1.36 and $I_{D'}/I_G$ of 0.45. At 1000 °C D and G bands have resembling intensities ($I_D/I_G = 0.98$), and at higher temperatures the intensity of the G band in all cases prevails on that of the D-band. Relative intensities of defect-related D and D' bands of graphite from reaction rims, which can be expressed as I_D/I_G and $I_{D'}/I_G$ ratios, demonstrate overall decrease with the temperature (Table 6). Particularly, I_D/I_G ratio decreases from 1.36 (900 °C) to 0.47 (1400 °C) and $I_{D'}/I_G$ decreases from 0.45 (900 °C) to 0.16 (1400 °C). The second-order G' band in this type of graphite, synthesized at 900 and 1000 °C, arises as one peak Raman feature, less-intense than D and D' bands (Table 6). As the temperature increases, the G'-band changes from a single peak to a two peaks feature (G'_1 and G'_2, Fig. 7). Raman spectra of the plate graphite crystals, synthesized in the temperature range of 1300–1600 °C, are characterized by very intense G band, and correspondingly low I_D/I_G ratios of 0.27–0.36 (without T dependence). A second-order G'-band is found to be a two peaks feature at all temperatures.

The diamond Raman spectra display a main diamond sp^3 peak at 1332 cm^{-1} and peaks indicative of inclusions related to carbonate, graphite and sulfide (Figs. 5, 6). Inclusions were formed both in carbide-carbonate-sulfur and iron-carbonate-sulfur systems, in the temperature range of 1400–1600 °C. Carbonate inclusions were identified by sharp peaks in ~1083–1097 cm^{-1} Raman region; they consisted of microdendrites of dolomite, aragonite and magnesite (Fig. 6a) in various proportions. These inclusions were trapped as carbonate melt during the early stages of the experiments, before carbonate melt was totally consumed. Inclusions of graphite were discovered in nearly all of the synthesized diamonds, their spectra were characterized by the main G-band at 1586 cm^{-1} (Fig. 5) and in some cases a defect-induced D' band at ~1620 cm^{-1}. Sulfide inclusions were characterized by main peaks at 215 and 279 cm^{-1} (pyrrhotite) as well as 347 and 381 cm^{-1} (pyrite) (Fig. 6b).

4. Discussion

At pressure of 6.3 GPa, sulfur occurs as a liquid at temperatures higher than 870°C (Brazhkin et al., 1999) (Fig. 2). Given the high volatility of sulfur, all carbide-carbonate-sulfur, iron-carbonate-sulfur interactions in a temperature range of 900–1600°C involve a sulfur melt/fluid.

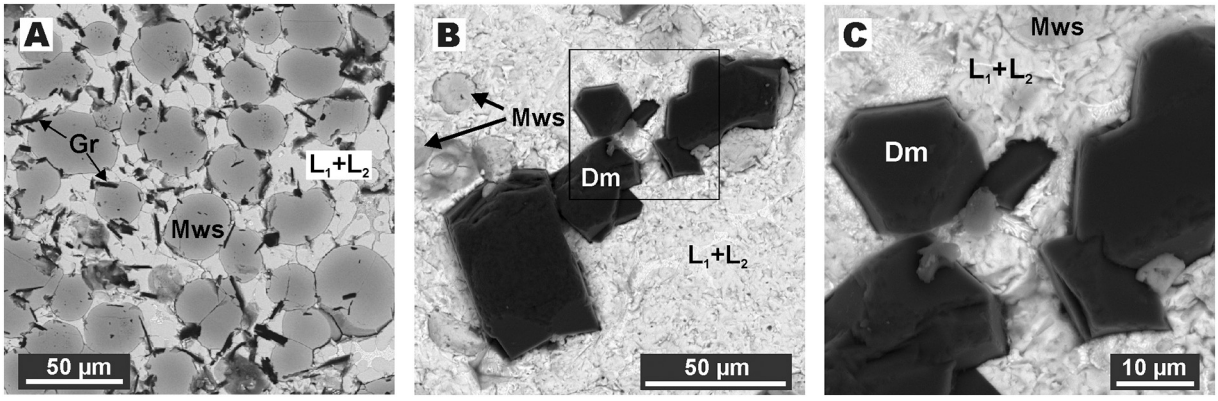

Fig. 3. SEM micrographs (BSE) of polished section (A) and cleaved surface (B, C) of the samples after experiments in metal-carbonate-sulfur system: A - rounded magnesiowüstite crystals and graphite plates in the quenched melts (1600 °C, N MSC-02). B - diamond and magnesiowüstite crystals in microdendritic metal-sulfide-oxide aggregates of quenched Fe-S-C and Fe-S-O melts (N MSC-98). C - enlarged fragment of Fig. 3B. Mws - magnesiowüstite, Gr - metastable graphite, Po - pyrrhotite, Coh - cohenite, L_1 - Fe-S-O melt, L_2 - Fe-S-C melt.

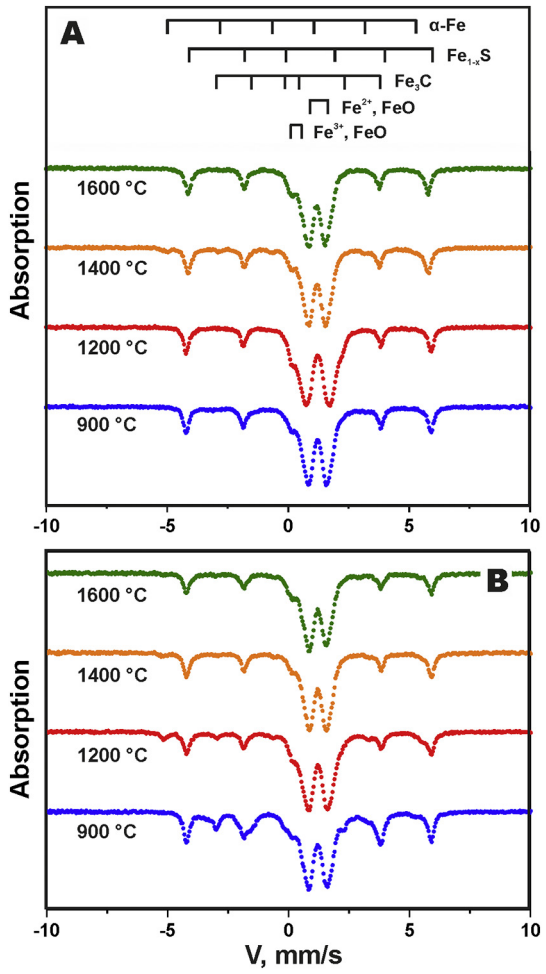

Fig. 4. Room-temperature Mössbauer spectra of representative samples from the metal-carbonate-sulfur system (A) and carbide-carbonate-sulfur system (B).

This melt/fluid can be considered in the first approximation as a model for natural reduced S-rich fluid, which is believed to be a powerful mantle metasomatic agent. Given our previous results on diamond and graphite formation via redox interactions of metallic iron + Mg,Ca-carbonate, and iron carbide + Mg,Ca-carbonate (P = 6.5–7.5 GPa, T = 1000–1650 °C, Palyanov et al., 2013), we may estimate the effect of a reduced S-rich fluid on these interactions. Modeling the interaction between carbonate and a reduced fluid rich in sulfur enables evaluating the carbon formation potential of this process.

4.1. Reconstruction of the main processes and mechanisms of graphite and diamond formation in the presence of reduced S-rich fluid

4.1.1. Graphite-forming processes in carbide-carbonate-sulfur system at subsolidus temperatures

At relatively low temperatures (900–1000°C), the main processes of elemental carbon (graphite) formation during the carbide-carbonate-sulfur interaction may be represented by the following reactions:

$$Fe_3C + 3S_{liquid} = 3FeS + C^0{}_{graphite} \quad (1)$$

$$3(Mg,Ca)CO_3 + Fe_3C = 3(Fe,Mg)O + 2C^0{}_{graphite} + 2CaCO_3 \quad (2)$$

$$MgCO_3 + Fe_3C + S_{liquid} = 3Fe_{0.66}\,Mg_{0.33}O + 2C^0{}_{graphite} + FeS \quad (3)$$

$$CaMg(CO_3)_2 + Fe_3C + S_{liquid} = CaCO_3 + 3Fe_{0.66}\,Mg_{0.33}O + 2C^0{}_{graphite} + FeS \quad (4)$$

The interaction between cohenite and a sulfur melt/fluid (1) is accompanied by extraction of carbon and iron from carbide and leads to the formation of pyrrhotite + graphite association and also to the formation of graphite rims around initial Fe_3C crystals. Analysis of the reaction structures preserved around single carbide grains demonstrated that the most likely mechanism for the formation of graphite is the extraction of carbon from carbide during the interaction with a sulfur melt. The redox reactions (2)–(4) describe processes of magnesite and dolomite reduction during the interaction with cohenite, which lead to crystallization of graphite in association with magnesiowüstite, pyrrhotite, and aragonite (Fig. 1a-d). It should be noted that graphite

Table 3
Compositions of oxide and carbonate phases, formed in the carbide-carbonate-sulfur and iron-carbonate-sulfur systems at P = 6.3 GPa, T = 900–1600°C and duration of 18–20 h (according to the microprobe analysis).

Run N	T, °C	Phase	N_A	Mass concentrations, wt%					N(O)	Cations per formula unit				
				FeO	MgO	CaO	CO_2	Total		Fe	Mg	Ca	C	Total
Fe_3C-$(Mg,Ca)CO_3$-S system														
CCS-23	900	Mws	14	$79_{(2)}$	$20_{(2)}$	$0.1_{(1)}$	–	$99.5_{(2)}$	1	$0.69_{(3)}$	$0.31_{(3)}$	–	–	$1.00_{(0)}$
		Ms	8	$1.5_{(1)}$	$43_{(2)}$	$0.1_{(1)}$	$55_{(2)}$	100.0	3	$0.02_{(0)}$	$0.90_{(5)}$	–	1.04(3)	$1.97_{(3)}$
		Dol	10	$0.9_{(3)}$	$20.4_{(12)}$	$28.4_{(4)}$	$49_{(2)}$	100.0	6	$0.02_{(1)}$	$0.93_{(7)}$	$0.94_{(3)}$	2.06(5)	$3.97_{(1)}$
		Arag	10	$1.0_{(5)}$	$0.1_{(0)}$	$52_{(1)}$	$46_{(1)}$	100.0	3	$0.01_{(1)}$	$0.002_{(1)}$	$0.98_{(2)}$	1.02(2)	$1.98_{(1)}$
CCS-03	1000	Mws	17	$83_{(2)}$	$15_{(2)}$	$0.3_{(1)}$	–	$99.3_{(1)}$	1	$0.75_{(3)}$	$0.25_{(3)}$	–	–	$1.00_{(0)}$
		Arag	12	$2.2_{(15)}$	$0.2_{(2)}$	$52_{(2)}$	$45_{(1)}$	100.0	3	$0.03_{(2)}$	$0.01_{(1)}$	$0.93_{(5)}$	1.02(2)	$1.98_{(2)}$
CCS-20	1100	Mws	15	$75.1_{(5)}$	$19.5_{(5)}$	$5.4_{(7)}$	–	$100.0_{(2)}$	1	$0.64_{(7)}$	$0.30_{(7)}$	$0.06_{(1)}$	–	$1.00_{(0)}$
CCS-19	1200	Mws	16	$76.2_{(1)}$	$18.6_{(1)}$	$5.2_{(3)}$	–	$100.0_{(4)}$	1	$0.66_{(1)}$	$0.29_{(1)}$	$0.06_{(0)}$	–	$1.01_{(0)}$
CCS-99	1300	Mws	15	$75.6_{(9)}$	$19.1_{(1)}$	$5.3_{(1)}$	–	$100.0_{(3)}$	1	$0.65_{(1)}$	$0.29_{(1)}$	$0.06_{(1)}$	–	$1.00_{(0)}$
CCS-18	1400	Mws	18	$72.2_{(2)}$	$21.8_{(2)}$	$6_{(1)}$	–	$100.0_{(3)}$	1	$0.61_{(3)}$	$0.33_{(3)}$	$0.06_{(1)}$	–	$1.00_{(0)}$
CCS-96	1500	Mws	18	$74.8_{(1)}$	$19.7_{(2)}$	$5.5_{(1)}$	–	$100.0_{(5)}$	1	$0.64_{(2)}$	$0.30_{(2)}$	$0.06_{(1)}$	–	$1.00_{(0)}$
CCS-02	1600	$Mws_{cen\ 1}$	1	61.4	32.7	5.2	–	99.3	1	0.49	0.46	0.05	–	1.00
		$Mws_{rim\ 1}$	1	95.7	3.8	–	–	99.5	1	0.93	0.07	–	–	1.00
		$Mws_{cen\ 2}$	1	60.5	33.7	5.2	–	99.3	1	0.48	0.47	0.05	–	1.00
		$Mws_{rim\ 2}$	1	86.1	13.7	–	–	99.8	1	0.78	0.22	–	–	1.00
Fe^0-$(Mg,Ca)CO_3$-S system														
MCS-98	1500	Mws_{cen}	14	$63.5_{(3)}$	$29.9_{(5)}$	$5.6_{(2)}$	–	$99.0_{(1)}$	1	$0.51_{(0)}$	$0.43_{(1)}$	$0.06_{(1)}$		$1.03_{(0)}$
		Mws_{rim}	14	$85.2_{(4)}$	$14.4_{(5)}$	–	–	$99.5_{(5)}$	1	$0.79_{(1)}$	$0.21_{(1)}$	–	–	$1.00_{(0)}$
MCS-02	1600	Mws_{cen}	14	$63.3_{(5)}$	$30.8_{(4)}$	$5.6_{(1)}$	–	$99.7_{(5)}$	1	$0.51_{(1)}$	$0.44_{(1)}$	$0.06_{(1)}$	–	$1.02_{(1)}$
		Mws_{rim}	14	$89.6_{(1)}$	$10.1_{(2)}$	–	–	$99.7_{(1)}$	1	$0.83_{(1)}$	$0.17_{(1)}$	–	–	$1.00_{(0)}$

Mws – magnesiowustite, Arg – aragonite, Ms – magnesite, Dol – dolomite, Carb – Fe,Mg,Ca-carbonate.

Table 4
Compositions of carbides, sulfides and melts, formed in the carbide-carbonate-sulfur and iron-carbonate-sulfur systems at P = 6.3 GPa, T = 900–1600°C and duration of 18–20 h (according to the microprobe analysis).

Run N	T, °C	Phase	N_A	Mass concentrations, wt%					Atomic proportions, at.%			
				Fe	S	C	O	Total	Fe	S	C	O
Fe_3C-(Mg,Ca)CO_3-S system												
CCS-23	900	Coh	8	$93.1_{(1)}$	–	$6.3_{(1)}$		$99.6_{(1)}$	$76.0_{(1)}$	–	$24.0_{(1)}$	–
		Po	10	$63.0_{(2)}$	$36.6_{(3)}$	–	–	$99.6_{(4)}$	$49.6_{(2)}$	$50.4_{(2)}$	–	–
CCS-03	1000	Coh	8	$93.1_{(1)}$	–	$6.3_{(1)}$	–	$99.6_{(1)}$	$76.0_{(1)}$	–	$24.0_{(1)}$	–
		Po	12	$64.0_{(4)}$	$35.6_{(2)}$	–	–	$99.6_{(3)}$	$50.7_{(3)}$	$49.3_{(3)}$	–	–
CCS-20	1100	Po	11	$63,2_{(4)}$	$36,5_{(1)}$	–	–	$99.7_{(2)}$	$49.8_{(1)}$	$50.0_{(1)}$	–	–
		$L_{Fe\text{-}S\text{-}O}$	24	$62.5_{(8)}$	$35.5_{(6)}$	–	$1.4_{(10)}$	$99.4_{(3)}$	$48.2_{(18)}$	$48.0_{(19)}$	–	$3.8_{(31)}$
		$L_{Fe\text{-}S\text{-}C}$	25	$78.8_{(4)}$	$20.1_{(4)}$	$0.6_{(5)}$	–	$99.6_{(3)}$	$67.5_{(15)}$	$30.2_{(8)}$	$2.4_{(22)}$	–
CCS-19	1200	$L_{Fe\text{-}S\text{-}O}$	27	$62.2_{(5)}$	$34.8_{(6)}$	–	$2.8_{(6)}$	$99.6_{(3)}$	$46.8_{(6)}$	$45.9_{(11)}$	–	$7.3_{(16)}$
		$L_{Fe\text{-}S\text{-}C}$	30	$76.8_{(3)}$	$21.8_{(3)}$	$1.0_{(0)}$	–	$99.5_{(4)}$	$64.2_{(3)}$	$31.9_{(3)}$	$3.9_{(1)}$	–
CCS-99	1300	$L_{Fe\text{-}S\text{-}O}$	24	$62.9_{(8)}$	$31.6_{(20)}$	–	$5.5_{(16)}$	$99.6_{(3)}$	$45.8_{(7)}$	$40.3_{(34)}$	–	$14.0_{(39)}$
		$L_{Fe\text{-}S\text{-}C}$	24	$75.9_{(19)}$	$21.4_{(16)}$	$2.3_{(8)}$	–	$99.5_{(2)}$	$61.3_{(32)}$	$30.2_{(19)}$	$8.6_{(3)}$	–
CCS-18	1400	$L_{Fe\text{-}S\text{-}O}$	25	$64.3_{(11)}$	$30.0_{(20)}$	–	$5.6_{(14)}$	$99.7_{(3)}$	$47.1_{(12)}$	$38.6_{(31)}$	–	$14.3_{(35)}$
		$L_{Fe\text{-}S\text{-}C}$	30	$77.8_{(15)}$	$19.1_{(17)}$	$2.8_{(6)}$	–	$99.4_{(3)}$	$62.6_{(22)}$	$27.0_{(23)}$	$10.4_{(22)}$	–
CCS-98	1500	$L_{Fe\text{-}S\text{-}O}$	24	$65.3_{(8)}$	$30.0_{(5)}$	–	$5.3_{(14)}$	$99.6_{(4)}$	$48.0_{(18)}$	$38.5_{(19)}$	–	$13.5_{(37)}$
		$L_{Fe\text{-}S\text{-}C}$	24	$77.9_{(7)}$	$18.2_{(6)}$	$3.1_{(4)}$	–	$99.9_{(3)}$	$62.8_{(17)}$	$25.6_{(19)}$	$11.6_{(18)}$	–
CCS-02	1600	$L_{Fe\text{-}S\text{-}O}$	24	$63.8_{(6)}$	$30.0_{(8)}$	–	$6.1_{(7)}$	$99.6_{(3)}$	$46.3_{(7)}$	$38.1_{(13)}$	–	$15.6_{(15)}$
		$L_{Fe\text{-}S\text{-}C}$	25	$78.2_{(10)}$	$18.8_{(10)}$	$2.5_{(3)}$	–	$99.5_{(3)}$	$63.7_{(16)}$	$26.7_{(11)}$	$9.6_{(10)}$	–
Fe^0-(Mg,Ca)CO_3-S system												
MCS-96	1500	$L_{Fe\text{-}S\text{-}O}$	28	$64.0_{(7)}$	$29.1_{(15)}$	–	$6.6_{(11)}$	$99.7_{(2)}$	$46.4_{(5)}$	$36.9_{(24)}$	–	$16.7_{(27)}$
		$L_{Fe\text{-}S\text{-}C}$	27	$75.9_{(3)}$	$22.2_{(2)}$	$1.7_{(6)}$	–	$99.8_{(6)}$	$61.9_{(17)}$	$31.6_{(6)}$	$6.5_{(23)}$	–
MCS-02	1600	$L_{Fe\text{-}S\text{-}O}$	30	$62.9_{(4)}$	$32.4_{(3)}$	–	$4.2_{(4)}$	$99.5_{(2)}$	$46.9_{(6)}$	$42.3_{(5)}$	–	$11_{(1)}$
		$L_{Fe\text{-}S\text{-}C}$	31	$74.8_{(7)}$	$22.4_{(5)}$	$2.2_{(1)}$	–	$99.3_{(2)}$	$60.3_{(6)}$	$31.6_{(7)}$	$8.1_{(4)}$	–

Po – pyrrhotite, Coh – cohenite, $L_{Fe\text{-}S\text{-}C}$ – Fe-S-C melt, $L_{Fe\text{-}S\text{-}O}$ – Fe-S-O melt; N_A - number of electron probe analyses used to obtain the average compositions. The values in parentheses are one sigma errors of the means based on replicate electron microprobe analyses reported as least units cited; $4.3_{(15)}$ should be read as 4.3 ± 1.5 wt%.

formed according to reactions (2)–(4) is always spatially confined to magnesiowüstite and occurs in inter-growths with it or in the form of inclusions (Fig. 1c), in contrast to graphite formed by reaction (1). In a simpler system (Mg,Ca)CO_3 + Fe_3C at P = 7.5 GPa and T = 1000–1100 °C (Palyanov et al., 2013), redox alkaline earth carbonate-cohenite interactions occur to form graphite, magnesiowüstite, and high-calcium carbonate according to reaction (2).

Table 5
^{57}Fe Mössbauer data for sulfides, carbide, metal and oxides.

Run N	T, °C	Phase	A, % (±2)
Fe_3C-(Mg,Ca)CO_3-S system			
CCS-23	900	$Fe_{1-x}S$, hexagonal, disordered vacancies	31
		$Fe_{1-x}S$, monoclinic, disordered vacancies	6
		Fe_3C	19
		FeO, Fe^{2+}	41
		FeO, Fe^{3+} (6)	3
CCS-20	1200	$Fe_{1-x}S$, hexagonal	28
		α-Fe	8
		FeO, Fe^{2+}	59
		FeO, Fe^{3+} (4)	5
CCS-18	1400	$Fe_{1-x}S$, hexagonal	33
		α-Fe	3
		FeO, Fe^{2+}	62
		FeO, Fe^{3+} (4)	3
CCS-02	1600	$Fe_{1-x}S$, hexagonal	30
		α-Fe	2
		FeO, Fe^{2+}	60
		FeO, Fe^{3+} (4)	8
Fe^0-(Mg,Ca)CO_3-S system			
MCS-02	1600	$Fe_{1-x}S$, hexagonal, defects	34
		FeO, Fe^{2+}	54
		FeO, Fe^{3+} (4)	7
		α-Fe, defects	5

IS – Isomer shift (mm/s) with reference to α-Fe; H – Magnetic hyperfine field; QS – Quadrupole splitting (mm/s); W – Width of the absorption line (mm/s); A – (Area(Fe^{3+})/(Area(Fe^{2+}) + Area(Fe^{3+})) × 100 or (Area(Fe^{2+})/(Area(Fe^{2+}) + Area(Fe^{3+})) × 100; Number in parenthesis - (4) or (6) denotes coordination number.

Therefore, reconstruction of processes of carbide-carbonate-sulfur interactions under subsolidus conditions has revealed that the main graphite-producing processes are extraction of iron from cohenite during interactions with the sulfur melt as well as the reduction of carbonate carbon during interactions of carbonate with Fe_3C. At relatively low temperatures, sulfur most likely has no decisive influence on crystallization of graphite in reactions (3) and (4), and its participation in the reactions is limited to crystallization of pyrrhotite, with a corresponding decrease in the iron content in magnesiowüstite.

4.1.2. Diamond- and graphite-forming processes involving Fe-S-C and Fe-S-O melts

Experiments in carbide-carbonate-sulfur and iron-carbonate-sulfur (Bataleva et al., 2016) systems demonstrate that significant differences in the interaction processes are observed only at relatively low temperatures, while under supersolidus conditions, very similar processes occur in the systems. We think that it is reasonable to present general reconstruction of diamond- and graphite-forming processes in both systems and indicate only the most significant differences.

We dwell on the most important issue of spontaneous diamond formation. Given our earlier results (Palyanov et al., 2013) the redox interaction of iron-carbonate and carbide-carbonate may be considered as one of the mechanisms of diamond formation in carbide-carbonate-sulfur and iron-carbonate-sulfur systems. At the early stages of relatively high-temperature experiments, spontaneous nucleation of diamond most likely occurs during redox reactions between carbide/metal and carbonate. At subsequent stages of the experiments, when carbonate is completely consumed, diamond growth and graphite formation occur via completely different mechanisms involving Fe-S-C and Fe-S-O melts, reconstruction of which is provided below.

There are well-documented immiscibility parameters between sulfur-rich and carbon-rich melts in the Fe-S-C based systems (e.g. Wood et al., 2014; Tsuno and Dasgupta, 2015; Zhang et al., 2018). Carbon solubility was demonstrated to increase with Metal/Sulfur ratio and dramatically decrease to negligible values when the Metal/Sulfur ratio gets close to 1. The partial melting onset temperature in carbide-carbonate-sulfur and iron-carbonate-sulfur systems was found to be

Table 6
Raman spectroscopy data of different types of graphite, synthesized in the carbide-carbonate-sulfur interaction.

Run N	T, °C	Type of graphite	First-order bands						Second-order bands				I_D/I_G	I_D/I_G	I_{G1}/I_D	I_{G1}/I_G
			D		G		D'		G'_1		D + G					
			RS	I	RS	I	RS	I	RS	I	RS	I				
CCS-23	900	Rim	1351	1529	1582	1124	1621	502	2706	401	2935	212	1.36	0.45	0.26	0.36
CCS-03	1000	Rim	1350	3835	1582	3909	1620	1322	2703	1242	2939	366	0.98	0.34	0.32	0.32
CCS-20	1100	Rim	1351	1385	1582	2052	1622	481	2717	795	2937	171	0.67	0.23	0.57	0.39
CCS-19	1200	Rim	1352	1127	1581	2045	1623	403	2718	766	2936	147	0.55	0.20	0.68	0.37
CCS-99	1300	Rim	1350	4376	1581	9183	1623	1394	2714	3393	2939	422	0.48	0.15	0.78	0.37
		Plate	1351	2991	1580	8051	1623	1101	2716	2696	2937	337	0.37	0.14	0.90	0.33
CCS-18	1400	Rim	1351	3824	1581	8085	1623	1306	2718	2868	2939	388	0.47	0.16	0.75	0.35
		Plate	1350	3826	1580	13,980	1622	1563	2718	4827	2940	452	0.27	0.11	1.26	0.35
CCS-96	1500	Plate	1348	2067	1579	5665	1621	832	2719	1993	2938	308	0.36	0.15	0.96	0.35
CCS-02	1600	Plate	1350	3776	1579	10,546	1619	2139	2718	3311	2937	499	0.36	0.20	0.88	0.31

RS – Raman shift (cm^{-1}), I – intensity (a.u.), I_D, I_G, $I_{D'}$, $I_{G'1}$ – intensities of D, G, D', G'_1 bands respectively. Notation of the Raman bands is after Pimenta et al., 2007.

1100 °C and 1300 °C, respectively. This temperature difference is most likely associated with the difference in bulk carbon concentrations in the systems: 8.1 wt% for the carbide-carbonate-sulfur system and 4.2 wt% for the iron-carbonate-sulfur system. Under these conditions, newly formed pyrrhotite melts, and the interaction between cohenite and the first portions of the sulfide melt occurs. This results in the enrichment of sulfide melt in iron and carbon, leading to the formation of a Fe-S-C melt. Simultaneously with this process, the sulfide melt also interacts with carbonate or carbonate melt to form a Fe-S-O melt and solid phase association of magnesiowüstite + graphite. The possibility of graphite (or diamond) crystallization during the reduction of carbonate by Fe—S and Fe-S-O melts was demonstrated earlier (Gunn and Luth, 2006; Palyanov et al., 2007). Therefore, upon complete melting of sulfide, these processes lead to the formation of a single *supersolidus* phase association represented by Fe-S-C and Fe-S-O melts, Fe^{3+}-bearing magnesiowüstite, and C^0.

An analysis of quenched melt aggregates (SEM, microprobe, Mössbauer) demonstrates that the Fe-S-O melt is a predominantly sulfide melt with dissolved FeO whose concentration in the melt, depending on the temperature, increases from 6 wt% (1100 °C) to 28 wt% (1600 °C). The Fe-S-C melt is found to be enriched in a metal-carbon (Fe—C) component. The Fe-S-C melt produced in the carbide-carbonate-sulfur system contains 38 to 46 wt% of Fe^0, 51 to 59 wt% of a sulfide component, and up to 3 wt% of dissolved carbon. Finally, the melt produced in the iron-carbonate-sulfur system contains 35 to 40 wt% of Fe^0, 57 to 62 wt% of Fe—S, and up to 3 wt% of C^0. In other words, the carbide-carbonate-sulfur and iron-carbonate-sulfur interactions lead to generation of two fO_2-contrasting melts, one of which contains Fe^{2+} (FeO), and the other contains metallic iron. Earlier, we demonstrated that the interaction between a metal-carbon melt and wüstite was a carbon-producing process accompanied by disproportionation of iron (Bataleva et al., 2016). In particular, oxidation of the metal-carbon melt by wüstite was found to be associated with the redox mechanism of graphite

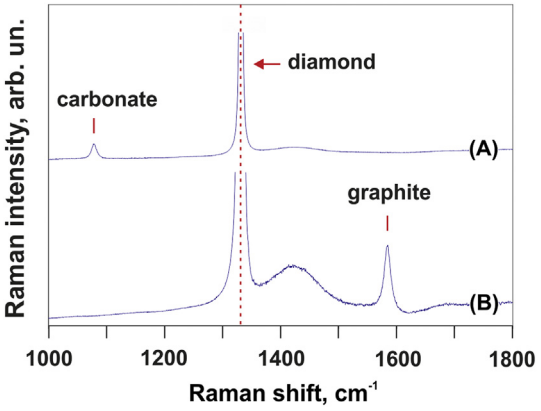

Fig. 5. Typical Raman spectra of the spontaneously nucleated diamonds formed via carbide-carbonate-sulfur (A) and iron-carbonate-sulfur interaction (B), as well as carbonate and graphite inclusions therein. Spectra are vertically displaced for clarity.

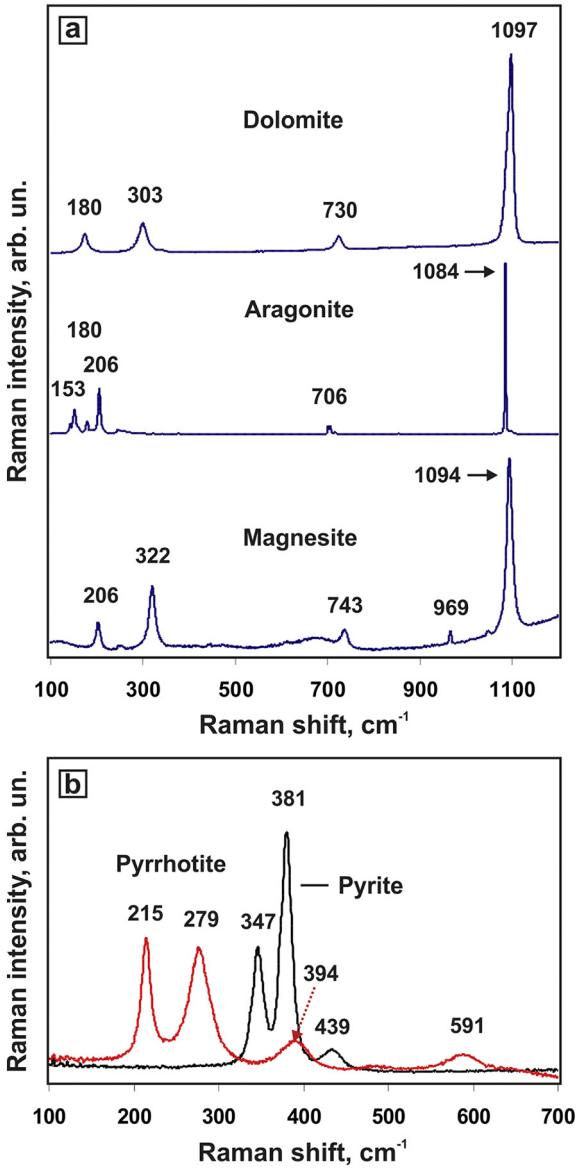

Fig. 6. Typical Raman spectra of carbonate (a) and sulfide (b) melt inclusions in diamonds (carbide-carbonate-sulfur interaction). Spectra are vertically displaced for clarity.

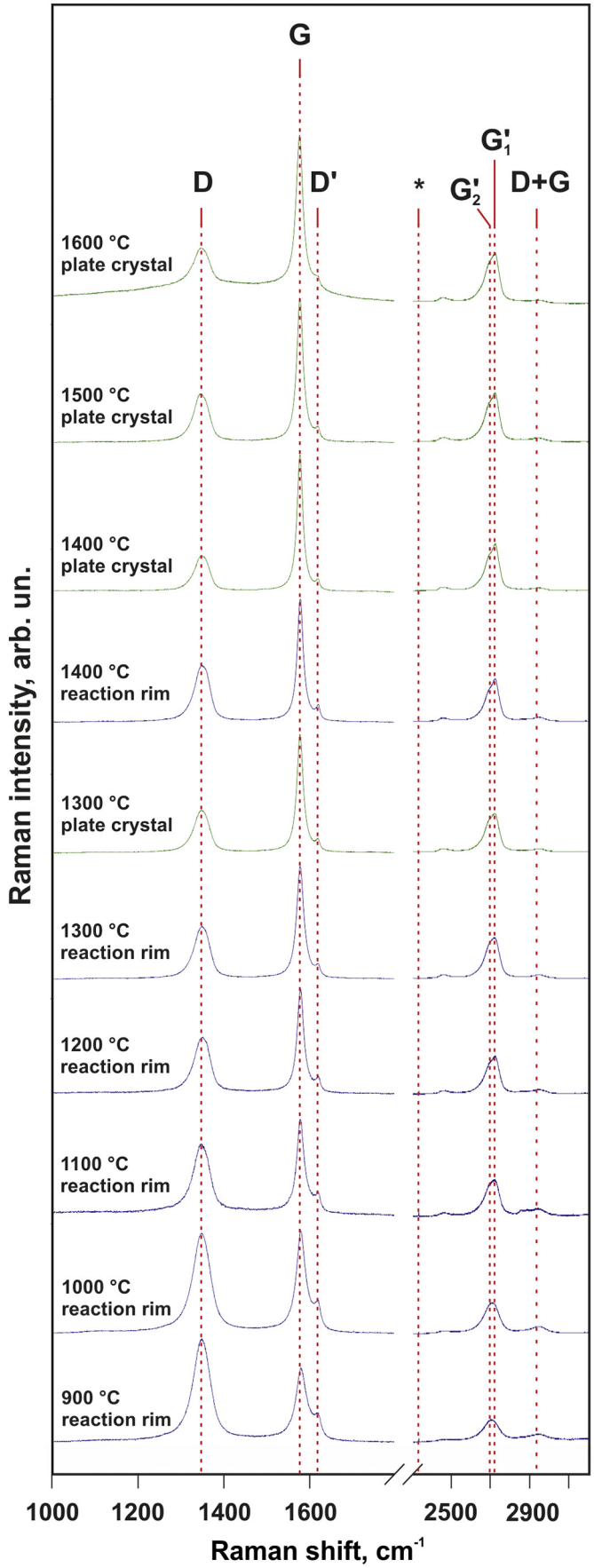

Fig. 7. Typical Raman spectra of graphite from reaction rim and single plate crystals (carbide-carbonate-sulfur interaction). Spectra are vertically displaced for clarity. Notations of the first-order and second-order bands are after Pimenta et al., 2007.

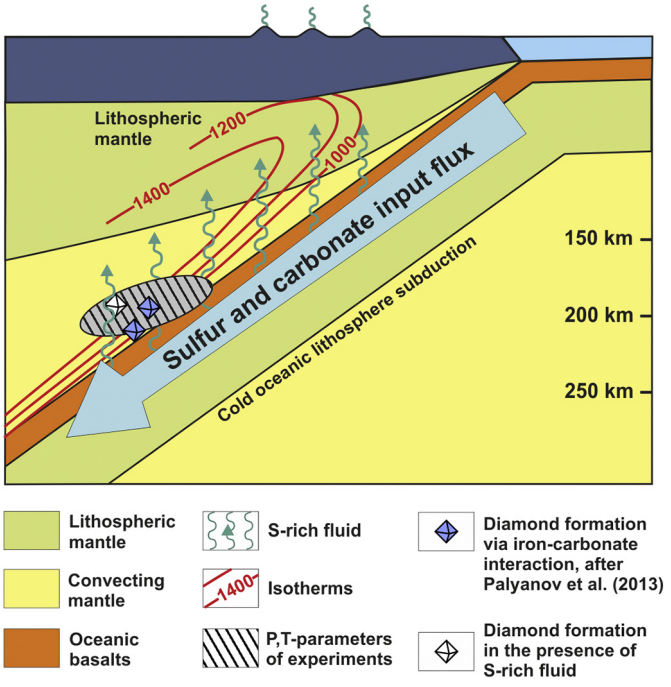

Fig. 8. Principal scheme and temperature features of a subduction zone based on data from Shirey et al. (2013) and Kogiso et al. (2009). Iron-carbonate interaction can result in the diamond formation at the P and T close to the slab/mantle boundary (Palyanov et al., 2013). Participation of sulfur-rich fluid in this interaction increases minimal temperatures of diamond formation by about 200 °C and shifts these processes to the mantle wedge.

crystallization and diamond growth with formation of the Fe^{3+}-bearing wüstite + graphite/diamond association. Despite the fact that samples produced in the present study lack reaction rims at the contact between Fe-S-O and Fe-S-C melts, direct evidence of their redox interaction is the formation of graphite and the grwoth of diamond directly in the Fe-S-C melt as well as the formation of Fe^{2+}- and Fe^{3+}-enriched magnesiowüstite rims at the contact with the Fe-S-O melt. It should be noted that graphite crystallization and diamond growth most likely occur due to both the redox interaction between melts with involvement of magnesiowüstite acting as a sink for Fe^{3+} and the interaction between the Fe-S-C melt and magnesiowüstite according to the schemes:

$$Fe{-}C_{(\text{in liquid})} + Fe{-}O_{(\text{in liquid})} = \left(Fe^{2+}, Fe^{3+}\right)O_{\text{solid}} + C^{0}{}_{\text{graphite,diamond}} \quad (5)$$

$$Fe{-}C_{(\text{in liquid})} + (Fe, Mg)O_{\text{solid}} = \left(Fe^{2+}, Fe^{3+}, Mg\right)O_{\text{solid}} + C^{0}{}_{\text{graphite,diamond}} \quad (6)$$

Thus, the diamond crystallization media and carbon source in these reactions is a metal-rich Fe-S-C melt. These processes occurring during Fe-S-C melt oxidation by the Fe-S-O melt and/or magnesiowüstite may be considered as the basis for reconstruction of the redox mechanism of graphite formation and diamond growth occurring during carbide-carbonate-sulfur and iron-carbonate-sulfur interactions.

A study by Palyanov et al. (2013) demonstrated that in redox-gradient experiments on the carbonate-iron interaction in reduced environments, diamond nucleation may occur in Fe—C melt pockets in the case of contact with graphite. As iron reacts with carbonate, the Fe—C melt is saturated with carbon, iron is consumed by oxidation, and further diamond growth proceeds under carbon supersaturation of the residual melt. At the final stage, the metal-carbon melt is completely consumed and replaced with diamond in the association with magnesiowüstite. It should be noted that the redox gradient was not created in a capsule in the present study, but it may occur locally,

and, under supersolidus conditions in the reaction volume. Carbon was present only as a part of the Fe-S-C melt, graphite, and diamond. Therefore, the Fe-S-C melt could not be enriched with carbon via reactions with the starting carbon-bearing phases (carbonate and carbide), and saturation of the melt with carbon occurred only through a decrease in the Fe^0 concentration in the melt, which was consumed through redox reactions. However, a decrease in the iron concentration in the Fe-S-C melt inevitably increases the sulfur concentration, which results in a number of consequences that should be considered in more detail.

An experimental study by Chepurov (1988), which was carried out in the Fe-S-C system at 5.0–5.5 GPa and in a temperature range of 1200–1500 °C, showed that introduction of sulfur into a transition metal melt sharply reduced the metallic melt reactivity (catalytic capacity) with respect to diamond and graphite. It was found that diamond nucleation could occur in S + metal melts, with the sulfur content being <35 at.%. In the present study, diamond growth was observed only in Fe-S-C melts with an atomic sulfur concentration of 26 to 27% for the carbide-carbonate-sulfur system and 31% for the iron-carbonate-sulfur system. At higher sulfur concentrations, only graphite crystallization occurred in the melt.

We should separately discuss potential effect of hydrogen diffusion on graphite/diamond formation. As it is known, during high-pressure high-temperature experiments, spontaneous diffusion of hydrogen occurs through the walls of Pt capsules (Brooker et al., 1998; Jakobsson and Oskarsson, 1994; Rosenbaum and Slagel, 1995) and Gr capsules as well. The reducing effect of hydrogen can be significant in case of high fO_2 values in the reaction volume. For example, diamond growth, due to partial reduction of CO_2 with H_2, was established in the $MgCO_3$-SiO_2-Al_2O_3 system at 6.0 GPa and 1600 °C (Pal'yanov et al., 2005). If the fO_2 values in the reaction volume are very low, in metal- or carbide-bearing systems, an effect of hydrogen is negligible.

Based on these observations, we propose a potential mechanism of diamond growth and graphite formation which involves carbide-carbonate-sulfur and iron-carbonate-sulfur interactions. In a temperature range of 1400–1600 °C, spontaneous nucleation of diamond occurs due to redox interactions between carbide or iron and carbonate, and further diamond growth occurs in a $Fe_{78}S_{19}C_3$-$Fe_{75}S_{22}C_2$ melt (subscripts indicate weight proportions). Oxidation of the Fe-S-C melt by the Fe-S-O melt and/or magnesiowüstite is accompanied by a decrease in the Fe^0 concentration in the Fe-S-C melt and by formation of highly ferrous and highly ferric magnesiowüstite. This process results in saturation of the Fe-S-C melt with carbon, which facilitates diamond growth and formation of metastable graphite. We suppose that at the final stage of this process, when the Fe—C component of the Fe-S-C melt is completely consumed, the phase assemblage in samples is represented by diamond, graphite, Fe^{3+}- magnesiowüstite, and a sulfide melt.

4.1.3. Raman characterization of graphite

As it is known, the most prominent features in the Raman spectra of graphite are the so-called G band appearing at 1560–1582 cm^{-1}, the D band at about 1350–1360 cm^{-1}, the D'-band at about 1620 cm^{-1} and the G'-band at about 2700 cm^{-1}. The first-order Raman bands of graphite are G, D and D'. The G band is the main peak arising due to the bond stretching of all pairs of sp^2 atoms and it appears in every Raman spectra of crystalline graphite. The D and D' are defect-induced Raman features, which cannot be seen in the spectra of highly crystalline graphite. The integrated intensity ratio for the D-band and G-band (I_D/I_G) is widely used for characterizing the defectiveness of graphite (e.g. Ferrari, 2007; Pimenta et al., 2007).

The results of Raman spectroscopy of graphite in the present study demonstrate that the relative intensities of defect-induced bands depend on the temperature and on graphite type (Fig. 6, Table 6). Graphite from the reaction rims around cohenite crystals at the lowest temperature is found to have the most defective structure with I_D/I_G ratio of 1.36 and $I_{D'}/I_G$ of 0.45. Since the I_D/I_G ratio was shown to be inversely proportional to the graphite crystallite sizes (Tuinstra and Koening, 1970), such spectra with intense D-band can be interpreted as a result of analysis of micro- or even nanocrystalline aggregates. On the whole, in the Raman spectra of graphite from reaction rims, the relative intensities of defect-related D and D' bands tend to overall decrease with the temperature (Table 6). However, we believe that these transformations of the structure of graphite are not directly temperature-dependent, but reflect the changes of crystallization mechanism from reactions (1)–(4) to (5)–(6). Correspondingly, the Raman spectra of the plate graphite crystals (1300–1600 °C), formed via reactions (5) and (6) are characterized by very intense G band and low I_D/I_G ratios that indicate highly crystalline graphite.

The most intense second-order Raman bands of graphite are G' and D + G ones (Pimenta et al., 2007). All kinds of graphitic materials display a strong Raman band appearing at 2500–2800 cm^{-1} and corresponding to the overtone of the D band. The Raman feature at about 2950 cm^{-1} is associated with a D + G combination mode and is also induced by disorder. In the present study, the second-order G' band in graphite rims (900 and 1000 °C) arises as one peak Raman feature. As the temperature increases, G'-band changes from one peak to a two peaks feature (G'_1 and G'_2, Fig. 6). For plate graphite crystals, G'-band is found to be a two peaks feature at all temperatures. It is known, that the change from one peak to two peaks in the profile of the G'-band in the Raman spectra can be caused by transformation from polycrystalline graphite to crystalline graphite (Nemanich and Solin, 1979), and temperature increase (Lespade et al., 1984). In these researches it is suggested that the origin of the two peaks structure of the G' band in crystalline graphite is related to the stacking order occurring along the *c* axis.

4.2. Main features of the influence of reduced S-rich fluid on diamond- and graphite-forming processes via carbide-carbonate or iron-carbonate interactions

Comparing the results obtained in carbide-carbonate-sulfur and iron-carbonate-sulfur systems with the results obtained in carbide-carbonate and iron-carbonate systems (Palyanov et al., 2013), we identified several features of the presence of a reduced S-rich fluid. In particular, these include a sharp decrease in the partial melting temperatures and reduced reactivity of the metal-carbon melt with respect to diamond crystallization. We will consider below the most distinctive effects that arise in the carbide-carbonate-sulfur system.

Experiments with the redox gradient (Palyanov et al., 2013), which were designed to study the carbide-carbonate interaction at P = 7.5 GPa and temperatures in a range of 1000–1400 °C, the formation of a solid phase association of cohenite + magnesiowüstite + graphite was found in a reduced part of samples. The authors identified and indicated a direct relationship between the absence of spontaneous diamond crystallization and the lack of a Fe—C melt. The present study revealed that addition of 10.7 wt% of sulfur to the carbide-carbonate system led to a reduction in the partial melting onset temperature in the system by at least 300 °C and to the formation of the first portions of Fe-S-C and Fe-S-O melts at T = 1100 °C (P = 6.3 GPa).

The data obtained by Tsuno and Dasgupta (2015) on the role of sulfur in carbon storage in the reduced, mid- to deep-upper mantle, confirmed that (i) dissolved S expands the stability field of metal-carbon melt to lower temperatures and (ii) C solubility in metal-carbon melt decreases with increasing S content. They showed that the presence of sulfide in the mantle ensures diamond stability even in C-depleted mantle as long as 100–200 ppm S is present. It was shown, that in S-depleted or S-free mantle, the stability of diamond requires higher bulk concentration of carbon. Based on these results, diamond, coexisting with Ni-rich sulfide liquid alloy is expected to be stable in the reduced, alloy-bearing oceanic mantle with C content as low as 5–20 ppm for mantle S varying between 100 and 200 ppm. In the study of Tsuno and Dasgupta Fe,Ni-alloy, carbon and sulfur were used as chemical reagents. Our research demonstrated that involvement of natural

carbonates as well as carbides results in the revealing of more complex regularities.

Another effect of sulfur on carbide-carbonate and metal-carbonate interactions is the reactivity of reduced metal-carbon melt with respect to diamond crystallization found by Chepurov (1988). Comparison of the results of experiments in sulfur-bearing and sulfur-free systems (Fig. 2) revealed an increase in the temperature of spontaneous diamond nucleation onset by ~200 °C in the presence of sulfur. In addition, growth rates of spontaneously formed diamond crystals in the $Fe_{75}S_{22}C_2$ (wt%) melt are approximately 10-folds lower than those in the Fe—C melt at comparable P and T. Therefore, the results of our experiments indicate that the presence of sulfur is able to decrease melting temperatures and widen the temperature field of stability of diamond-producing, predominantly metal melts. Furthermore, sulfur reduces the diamond-forming ability of metal-carbon melts and, at high S concentration, can completely inhibit diamond nucleation and crystallization.

Based on previous experimental studies aiming at modeling the crystallization of diamond in various natural environments systems, we can highlight some of the possible effects of the individual chemical components on the parameters of the diamond-forming processes. In particular, under subduction conditions, it is most likely that an aqueous fluid should be present. According to experimental data, the presence of water or H_2O-CO_2 fluid significantly reduces the temperature of generation of carbonate melts (e.g. Shatskiy et al., 2013) and greatly increases the diamond-forming ability of carbonate-bearing mantle fluids or melts. On the other hand, it was experimentally demonstrated that, under reduced mantle conditions where diamond crystallizes from the metal-carbon melt, the presence of H_2O will lead to an inhibitory effect on the diamond-forming process (Palyanov et al., 2012). More specifically, it has been shown that ~ 0.48 wt% H_2O admixture in the Fe-Ni-C melt is sufficient for the formation of metastable graphite in the thermodynamic stability field of diamond.

4.3. Diamond formation via carbide-carbonate-sulfur or iron-carbonate-sulfur interactions in natural environments

In the recent decades it has been generally agreed that most lithospheric diamonds grew in the mantle during metasomatic events, from a carbon-rich fluid or carbonate-based melts (see reviews Taylor and Anand, 2004; Shirey et al., 2013; Cartigny et al., 2014). This idea is confirmed by the presence of carbonate inclusions in diamonds of different depths of origin and ages (Brenker et al., 2007; Kaminsky et al., 2013; Logvinova et al., 2015; Stachel et al., 1998; Wang et al., 1996; Wirth et al., 2009). Moreover, numerous experimental studies have confirmed the possibility that carbonate melts are the predominant sources of carbon in diamond formation processes. Some of the carbonate melts or fluids in the mantle are considered to be of subduction-related origin. They have a specific carbon isotope ($\delta^{13}C$) crustal signatures which can be inherited by diamonds and inclusions therein. For example, this crustal signature is characteristic in some of the E-type diamonds ($\delta^{13}C$ values from +3‰ to −35‰) (Sobolev and Sobolev, 1980; Deines et al., 2001a, 2001b) and ultra deep diamonds ($\delta^{13}C$ values of −23‰) (Ickert et al., 2015). As it is well known, the most common mineral inclusions in the lithospheric diamonds are silicates (Cr-pyrope, diopside, enstatite and olivine for peridotitic paragenesis; pyrope-almandine, omphacite, coesite and kyanite for eclogitic paragenesis) and sulfides (monosulfide solid solution, pentlandite, Ni-rich pyrrhotite for peridotitic paragenesis; Ni-poor or Ni-free pyrrhotite and pyrite-pyrrhotite assemblages for eclogitic paragenesis). Among subduction signatures from inclusions in diamonds there are specific stable isotope compositions of oxygen ($\delta^{18}O$ values from +3‰ to more than +12‰) and sulfur ($\delta^{34}S$ values from −5‰ to +6‰) in silicate and sulfide inclusions (Cartigny et al., 2014 and references therein).

The most valuable data on the diamond genesis can be gathered from inclusions that have been identified in their genetic centers (Bulanova, 1995). Particularly, “central” inclusions of both peridotitic and eclogitic suites of Yakutian diamonds are typically represented by the silicate + sulfide + graphite assemblage. However, it was shown that Yakutian lithospheric diamonds of unknown paragenesis have “central” inclusions with mineral assemblages of native iron, cohenite, pyrrhotite, wüstite, and graphite, which indicate that the redox conditions of formation of these diamonds corresponded to the iron-wüstite buffer. Moreover, this assemblage was considered to be a catalyst for the process of diamond nucleation. According to the present study, exactly the same assemblage can be formed as a result of diamond-forming redox interactions of carbonate with carbide or native iron in the presence of sulfur-rich reduced fluid. Since the presence of sulfur increases the temperatures of diamond formation to the values higher than supposed to be in the down going slab (Fig. 8), this interaction can be realized in the mantle wedge as a result of metasomatic alteration of reduced mantle rocks by mobile, subduction-related, carbonate-bearing melts and S-rich fluids.

5. Conclusions

1) In a course of carbide-carbonate-sulfur and iron-carbonate-sulfur interactions at a pressure of 6.3 GPa, metastable graphite crystallization (900–1600 °C) and spontaneous diamond formation (1400–1600 °C) were realized.
2) At the subsolidus temperatures in the carbide-carbonate-sulfur system (T < 1100 °C), extraction of carbon from cohenite through the interaction with S-rich reduced fluid, as well as C^0-producing redox reactions of carbonate with carbide or iron were found to occur. Under these conditions graphite formation in assemblage with magnesiowüstite and pyrrhotite (±aragonite) was established.
3) At the supersolidus temperatures formation of Fe^{3+}- magnesiowüstite +graphite (1100–1600 °C) or Fe^{3+}- magnesiowüstite+graphite+diamond (1400–1600 °C) assemblages was accompanied by generation of fO_2-contrasting metal-sulfide with dissolved carbon (Fe-S-C) and sulfide-oxide (Fe-S-O) melts. It was found, that redox interactions of Fe-S-C and Fe-S-O melts with participation of magnesiowüstite, were a diamond-forming process, accompanied by disproportionation of Fe. Spontaneous diamond nucleation was found to occur via redox interactions of carbide or iron with carbonate.
4) It was established that the main features of the presence of S-rich reduced fluid in the course of carbide-carbonate or iron-carbonate interactions are a sharp decrease of partial melting temperatures by ~300 °C, an increase of the temperature of arising of spontaneous diamond nucleation by at least 200 °C and a decrease of diamond growth rate.

Asknowledgements

This work was supported by the Russian Science Foundation under Grant No. 14–27–00054 and a state assignment of IGM SB RAS. The authors thank S. Ovchinnikov for his assistance in implementation of the Mössbauer spectroscopy measurements.

References

Akaishi, M., Kanda, H., Yamaoka, S., 1990. Synthesis of diamond from graphite-carbonate systems under very high temperature and pressure. Journal of Crystal Growth 104, 578–581.

Ballhaus, C., 1995. Is the upper mantle metal-saturated? Earth and Planetary Science Letters 132, 75–86. https://doi.org/10.1016/0012-821X(95)00047-G.

Bataleva, Yu.V., Palyanov, Yu.N., Borzdov, Yu.M., Bayukov, O.A., Sobolev, N.V., 2016. The formation of graphite upon the interaction of subducted carbonates and sulfur with metal-bearing rocks of the lithospheric mantle. Doklady Earth Sciences 466 (1), 88–91. https://doi.org/10.1134/S1028334X16010190.

Bataleva, Y.V., Palyanov, Y.N., Borzdov, Y.M., Bayukov, O.A., Zdrokov, E.V., 2017. Iron carbide as a source of carbon for graphite and diamond formation under lithospheric mantle P-T parameters. Lithos 286-287, 151–161. https://doi.org/10.1016/j.lithos.2017.06.010.

Boehler, R., 1992. Melting of the Fe-FeO and the Fe-FeS systems at high pressure – constraints on core temperatures. Earth and Planetary Science Letters 111, 217–227. https://doi.org/10.1016/0012-821X(92)90180-4.
Brazhkin, V.V., Popova, S.V., Voloshin, R.N., 1999. Pressure-temperature phase diagram of molten elements: selenium, sulfur and iodine. Physica B, Condensed Matter 265, 64–71. https://doi.org/10.1016/S0921-4526(98)01318-0.
Brenker, F.E., Vollmer, C., Vincze, L., Vekemans, B., Szymanski, A., Janssens, K., Szaloki, I., Nasdala, L., Joswig, W., Kaminsky, F., 2007. Carbonates from the lower part of transition zone or even the lower mantle. Earth and Planetary Science Letters 260, 1–9. https://doi.org/10.1016/j.epsl.2007.02.038.
Brooker, R., Holloway, J.R., Hervig, R., 1998. Reduction in piston-cylinder experiments: the detection of carbon infiltration into platinum capsules. American Mineralogist 83, 985–994.
Bulanova, G.P., 1995. The formation of diamond. Journal of Geochemical Exploration 53, 2–23. https://doi.org/10.1016/0375-6742(94)00016-5.
Bureau, H., Remusat, L., Esteve, M., Pinti, D., Cartigny, P., 2018. The growth of lithospheric diamonds. Science Advances 4 (6), eaat1602. https://doi.org/10.1126/sciadv.aat1602.
Cartigny, P., Palot, M., Thomassot, E., Harris, J.W., 2014. Diamond formation: a stable isotope perspective. Annual Review of Earth and Planetary Sciences 42, 699–732. https://doi.org/10.1146/annurev-earth-042711-105259.
Chepurov, A.I., 1988. The role of sulfide melt in the process of natural diamond formation. Geologiya i Geofizika (Soviet Geology and Geophysics) 29 (8, 119–124 (112–116)).
Dasgupta, R., Hirschmann, M.M., 2010. The deep carbon cycle and melting in Earth's interior. Earth and Planetary Science Letters 298, 1–13. https://doi.org/10.1016/j.epsl.2010.06.039.
Deines, P., Harris, J.W., 1995. Sulfide inclusion chemistry and carbon isotopes of African diamonds. Geochimica et Cosmochimica Acta 59 (15), 3173–3188. https://doi.org/10.1016/0016-7037(95)00205-E.
Deines, P., Vilijoen, F., Harris, J.W., 2001a. Implications of the carbon isotope and mineral inclusion record for the formation of diamonds in the mantle underlying a mobile belt: Venetia, South Africa. Geochimica et Cosmochimica Acta 65 (5), 813–838. https://doi.org/10.1016/S0016-7037(00)00569-X.
Deines, P., Viljoen, F., Harris, J.W., 2001b. Implications of the carbon isotope and mineral inclusion record for the formation of diamonds in the mantle underlying a mobile belt: Venetia, South Africa. Geochimica Cosmochimica Acta 65, 813–838. https://doi.org/10.1016/S0016-7037(00)00569-X.
Dilek, Y., Yang, J., 2018. Ophiolites, diamonds, and ultrahigh-pressure minerals: New discoveries and concepts on upper mantle petrogenesis. Lithosphere 10, 3–13. https://doi.org/10.1130/L715.1.
Dobrzhinetskaya, L.F., Wirth, R., Green, Harry W., 2007. A look inside of diamond-forming media in deep subduction zones. Proceedings of the National Academy of Sciences of the United States of America 104 (22), 9128–9132. https://doi.org/10.1073/pnas.0609161104.
Eggler, D.H., Lorand, J.P., 1993. Mantle sulfide geobarometry. Geochimica et Cosmochimica Acta 57, 2213–2222. https://doi.org/10.1016/0016-7037(93)90563-C.
Evans, K.A., 2012. The redox budget of subduction zones. Earth-Science Reviews 113, 11–32. https://doi.org/10.1016/j.earscirev.2012.03.003.
Ferrari, A.C., 2007. Raman spectroscopy of graphene and graphite: disorder, electron-phonon coupling, doping and nonadiabatic effects. Solid State Communications 143, 47–57. https://doi.org/10.1016/j.ssc.2007.03.052.
Frost, D.J., McCammon, C.A., 2008. The redox state of Earth's mantle. Annual Review of Earth and Planetary Sciences 36, 389–420. https://doi.org/10.1146/annurev.earth.36.031207.124322.
Girnis, A.V., Brey, G., Bulatov, V.K., Höfer, H., Woodland, A.B., 2018. Graphite to diamond transformation during sediment–peridotite interaction at 7.5 and 10.5 GPa. Lithos 310, 302–313. https://doi.org/10.1016/j.lithos.2018.04.010.
Gunn, S.C., Luth, R.W., 2006. Carbonate reduction by Fe-S-O melts at high pressure and high temperature. American Mineralogist 91, 1110–1116. https://doi.org/10.2138/am.2006.2009.
Haggerty, S.E., 1986. Diamond genesis in a multiply constrained model. Nature 320, 34–48. https://doi.org/10.1038/320034a0.
Ickert, R.B., Stachel, T., Stern, R.A., Harris, J.W., 2015. Extreme ^{18}O-enrichment in majorite constrains a crustal origin of transition zone diamonds. Geochemical Perspectives Letters 1 (1). https://doi.org/10.7185/geochemlet.1507.
Jakobsson, S., Oskarsson, N., 1994. The system C–O in equilibrium with graphite at high pressure and temperature: an experimental study. Geochimica et Cosmochimica Acta 58, 9–17.
Kaminsky, F., Wirth, R., Schreiber, A., 2013. Carbonatitic inclusions in deep mantle diamond from Juina, Brazil: new minerals in the carbonate-halide association. The Canadian Mineralogist 51, 669–688. https://doi.org/10.3749/canmin.51.5.669.
Kennedy, C.S., Kennedy, G.C., 1976. The equilibrium boundary between graphite and diamond. Journal of Geophysical Research 81, 2467–2470.
Kogiso, T., Omori, S., Maruyama, S., 2009. Magma genesis beneath Northeast Japan arc: A new perspective on subduction zone magmatism. Gondwana Res. 16, 446–457. https://doi.org/10.1016/j.gr.2009.05.006.
Kogiso, T., Omori, S., Maruyama, S., 2009. Magma genesis beneath Northeast Japan arc: A new perspective on subduction zone magmatism. Gondwana Research 16, 446-457, doi: 10.1016/j.gr.2009.05.006. Lespade, P., Marchard, A., Couzi, M., Cruege, F., 1984. Caracterisation de materiaux carbones par microspectrometrie Raman. Carbon 22, 375–385. https://doi.org/10.1016/0008-6223(84)90009-5.
Litvin, Yu.A., Butvina, V.G., Bobrov, A.V., Zharikov, V.A., 2002. The first synthesis of diamond in sulfide-carbon systems: the role of sulfides in diamond genesis. Doklady Earth Sciences 382, 40–43.
Logvinova, A.M., Fedorova, E.N., Yelisseyev, A.P., Reutsky, V.N., Sobolev, N.V., Taylor, L.A., Wirth, R., Howarth, G., 2015. A unique diamondiferous peridotite xenolith from the Udachnaya kimberlite pipe, Yakutia: role of subduction in diamond formation. Russian Geology and Geophysics 56 (1–2), 306–320. https://doi.org/10.1016/j.rgg.2015.01.022.
Luth, R.W., 1999. Carbon and carbonates in mantle. In: Fei, Y., Bertka, M.C., Mysen, B.O. (Eds.), Mantle Petrology: Field Observation and High Pressure Experimentation: A Tribute to Francis R. (Joe) Boyd. The Geochemical Society, Special Publication, No. 6, pp. 297–316.
Marx, P.C., 1972. Pyrrhotine and the origin of terrestrial diamonds. Mineralogical Magazine 38, 636–638.
Meyer, H.O.A., Svicero, D.P., 1975. Mineral inclusions in Brazilian diamonds. Physics and Chemistry of the Earth 9, 785–795. https://doi.org/10.1016/0079-1946(75)90051-8.
Nemanich, R.J., Solin, S.A., 1979. First- and second-order Raman scattering from finite-size crystals of graphite. Physical Review B 20, 392. https://doi.org/10.1103/PhysRevB.20.392.
Oganov, A.R., Ono, S., Ma, Y., Glass, C.V., Garcia, A., 2008. Novel high-pressure structures of $MgCO_3$, $CaCO_3$ and CO_2 and their role in Earth's lower mantle. Earth and Planetary Science Letters 273, 38–47. https://doi.org/10.1016/j.epsl.2008.06.005.
Palyanov, Yu.N., Borzdov, Yu.M., Khokhryakov, A.F., Kupriyanov, I.N., Sobolev, N.V., 2006. Sulfide melts-graphite interaction at HPHT conditions: Implications for diamond genesis. Earth and Planetary Science Letters 250, 269–280. https://doi.org/10.1016/j.epsl.2006.06.049.
Palyanov, Y.N., Borzdov, Y.M., Bataleva, Y.V., Sokol, A.G., Palyanova, G.A., Kupriyanov, I.N., 2007. Reducing role of sulfides and diamond formation in the Earth's mantle. Earth and Planetary Science Letters 260 (1–2), 242–256. https://doi.org/10.1016/j.epsl.2007.05.033.
Palyanov, Y.N., Borzdov, Y.M., Kupriyanov, I.N., Khokhryakov, A.F., 2012. Effect of H_2O on diamond crystal growth in metal–carbon systems. Crystal Growth & Design 12, 5571–5578. https://doi.org/10.1021/cg301111g.
Palyanov, Y.N., Bataleva, Y.V., Sokol, A.G., Borzdov, Y.M., Kupriyanov, I.N., Reutsky, V.N., Sobolev, N.V., 2013. Mantle–slab interaction and redox mechanism of diamond formation. Proceedings of the National Academy of Sciences of the USA 110 (51), 20408–20413. https://doi.org/10.1073/pnas.1313340110.
Pal'yanov, Y., Borzdov, Y., Kupriyanov, I., Gusev, V., Khokhryakov, A., Sokol, A., 2001. High-pressure synthesis and characterization of diamond from a sulfur-carbon system. Diamond and Related Materials 10, 2145–2152. https://doi.org/10.1016/S0925-9635(01)00494-0.
Pal'yanov, Y.N., Sokol, A.G., Borzdov, Y.M., Khokhryakov, A.F., 2002. Fluid-bearing alkaline carbonate melts as the medium for the formation of diamonds in the Earth's mantle: an experimental study. Lithos 60 (3–4), 145–159. https://doi.org/10.1016/S0024-4937(01)00079-2.
Pal'yanov, Yu.N., Sokol, A.G., Tomilenko, A.A., Sobolev, N.V., 2005. Conditions of diamond formation through carbonate-silicate interaction. European Journal of Mineralogy 17, 207–214. https://doi.org/10.1127/0935-1221/2005/0017-0207.
Pimenta, M.A., Dresselhaus, G., Dresselhaus, M.S., Cançado, L.G., 2007. Studying disorder in graphite-based systems by Raman spectroscopy. Physical Chemistry Chemical Physics 9, 1276–1291. https://doi.org/10.1039/b613962k.
Rohrbach, A., Schmidt, M.W., 2011. Redox freezing and melting in the Earth's deep mantle resulting from carbon – iron redox coupling. Nature 472, 209–212. https://doi.org/10.1038/nature09899.
Rohrbach, A., Ballhaus, C., Golla-Schindler, U., Ulmer, P., Kamenetsky, V.S., Kuzmin, D.V., 2007. Metal saturation in the upper mantle. Nature 449, 456–458. https://doi.org/10.1038/nature06183.
Rosenbaum, J.M., Slagel, M.M., 1995. C–O–H speciation in piston-cylinder experiments. American Mineralogist 80, 109–114.
Sato, K., Katsura, T., 2001. Sulfur: a new solvent-catalyst for diamond synthesis under high-pressure and high-temperature conditions. Journal of Crystal Growth 223, 189–194.
Sato, K., Akaishi, M., Yamaoka, S., 1999. Spontaneous nucleation of diamond in the system $MgCO_3$-$CaCO_3$-C at 7.7 GPa. Diamond and Related Materials 8, 1900–1905. https://doi.org/10.1016/S0925-9635(99)00157-0.
Schissel, D., Smail, R., 2001. Deep-mantle plumes and ore deposits. GSA Special Papers 2001. vol. 352, pp. 291–322. https://doi.org/10.1130/0-8137-2352-3.291.
Sharp, W.E., 1966. Pyrrhotite: a common inclusion in South African diamonds. Nature 211, 402–403. https://doi.org/10.1038/211402b0.
Sharp, W.E., 1969. Melting curves of sphalerite, galena, and pyrrhotite and the decomposition curve of pyrite between 30 and 65 kilobars. Journal of Geophysical Research 74, 1645–1652. https://doi.org/10.1029/JB074i006p01645.
Shatskiy, A., Gavryushkin, P.N., Sharygin, I.S., Litasov, K.D., Kupriyanov, I.N., Higo, Y., Borzdov, Y.M., Funakoshi, K., Palyanov, Y.N., Ohtani, E., 2013. Melting and subsolidus phase relations in the system Na_2CO_3-$MgCO_3$ +/−H_2O at 6 GPa and the stability of $Na_2Mg(CO_3)_2$ in the upper mantle. American Mineralogist 98 (11−12), 2172–2182. https://doi.org/10.2138/am.2013.4418.
Shirey, S.B., Cartigny, P., Frost, D.G., Keshav, S., Nestola, F., Nimis, P., Pearson, D.G., Sobolev, N.V., Walter, M.J., 2013. Diamonds and the geology of mantle carbon. Reviews in Mineralogy and Geochemistry 75, 355–421. https://doi.org/10.2138/rmg.2013.75.12.
Smith, E.M., Shirey, S.B., Nestola, F., Bullock, E.S., Wang, J., Richardson, S.H., Wang, W., 2016. Large gem diamonds from metallic liquid in Earth's deep mantle. Science 354 (6318), 1403–1405. https://doi.org/10.1126/science.aal1303.
Sobolev, N.V., 1977. The Deep-Seated Inclusions in Kimberlites and the Problem of the Composition of the Upper Mantle. American Geophysics Union, Washington.
Sobolev, V.S., Sobolev, N.V., 1980. New evidence of the sinking to great depths of the eclogitized rocks of Earth crust. Doklady Akademii Nauk SSSR 250 (3), 683–685.
Sobolev, N.V., Efimova, E.S., Pospelova, L.N., 1981. Native iron in Yakutian diamonds and its paragenesis. Soviet Geology and Geophysics 22 (12), 18–21.
Sokol, A.G., Borzdov, Y.M., Palyanov, Y.N., Khokhryakov, A.F., 2015. High-temperature calibration of a multi-anvil high pressure apparatus. High Pressure Research 35 (2), 139–147. https://doi.org/10.1080/08957959.2015.1017819.

Stachel, T., Harris, J.W., Brey, G.P., 1998. Rare and unusual mineral inclusions in diamonds from Mwadui, Tanzania. Contributions to Mineralogy and Petrology 132 (1), 34–47. https://doi.org/10.1007/s004100050403.

Stagno, V., Tange, Y., Miyajima, N., McCammon, C.A., Irifune, T., Frost, D.J., 2011. The stability of magnesite in thetransition zone and the lower mantle as function of oxygen fugacity. Geophysical Research Letters 38. https://doi.org/10.1029/2011GL049560 L19309, 5 pp.

Taniguchi, T., Dobson, D., Jones, A.P., Rabe, R., Milledge, H.J., 1996. Synthesis of cubic diamonds in the graphite–magnesium carbonate and graphite–$K_2Mg(CO_3)_2$ systems at high pressure of 9–10 GPa region. Journal of Materials Research 11, 2622–2632.

Taylor, L.A., Anand, M., 2004. Diamonds: time capsules from the Siberian Mantle. Chemie der Erde 64, 1–74. https://doi.org/10.1016/j.chemer.2003.11.006.

Tsuno, K., Dasgupta, R., 2015. Fe-Ni-Cu-C-S phase relations at high pressures and temperatures-The role of sulfur in carbon storage and diamond stability at mid- to deep-upper mantle. Earth Planetary Sci. Lett. 412, 132–142. https://doi.org/10.1016/j.epsl.2014.12.018.

Tuinstra, F., Koening, J.L., 1970. Raman spectrum of graphite. The Journal of Chemical Physics 53, 1126. https://doi.org/10.1063/1.1674108.

Walter, M.J., Kohn, S.C., Araujo, D., Bulanova, G.P., Smith, C.B., Gaillou, E., Wang, J., Steele, A., Shirey, S.B., 2011. Deep mantle cycling of oceanic crust: evidence from diamonds and their mineral inclusions. Science 334 (6052), 54–57. https://doi.org/10.1126/science.1209300.

Wang, A., Pasteris, J.D., Meyer, H.O.A., DeleDuboi, M.L., 1996. Magnesite-bearing inclusion assemblage in natural diamond. Earth and Planetary Science Letters 141 (1–4), 293–306. https://doi.org/10.1016/0012-821X(96)00053-2.

Wentorf, R.H., 1974. Diamond formation at high pressures. In: Wentorf, R.H. (Ed.), Adv. in High Press, Research. Diamond Synthesis vol. 4, pp. 249–281.

Wirth, R., Kaminsky, F., Matsyuk, S., Schreiber, A., 2009. Unusual micro- and nano-inclusions in diamonds from the Juina Area, Brazil. Earth and Planetary Science Letters 286, 292–303. https://doi.org/10.1016/j.epsl.2009.06.043.

Wood, B.J., Kiseeva, E.S., Mirolo, F.J., 2014. Accretion and core formation: the effects of sulfur on metal–silicate partition coefficients. Geochimica et Cosmochimica Acta 145, 248–267. https://doi.org/10.1016/j.gca.2014.09.002.

Woodland, A.B., Koch, M., 2003. Variation in oxygen fugacity with depth in the upper mantle beneath the Kaapvaal craton, Southern Africa. Earth and Planetary Science Letters 214, 295–310. https://doi.org/10.1016/S0012-821X(03)00379-0.

Yaxley, G.M., Green, D.H., 1994. Experimental demonstration of refractory carbonate-bearing eclogite and siliceous melt in the subduction regime. Earth and Planetary Science Letters 128, 313–325. https://doi.org/10.1016/0012-821X(94)90153-8.

Zhang, Z., Hastings, P., Von der Handt, A., Hirschmann, M.M., 2018. Experimental determination of carbon solubility in Fe-Ni-S melts. Geochimica et Cosmochimica Acta 225, 66–79. https://doi.org/10.1016/j.gca.2018.01.009.